Suess, E., von Huene, R., et al., 1990
Proceedings of the Ocean Drilling Program, Scientific Results, Vol. 112

22. UPWELLING OFF PERU DURING THE LAST 430,000 YR AND ITS RELATIONSHIP TO THE BOTTOM-WATER ENVIRONMENT, AS DEDUCED FROM COARSE GRAIN-SIZE DISTRIBUTIONS AND ANALYSES OF BENTHIC FORAMINIFERS AT HOLES 679D, 680B, AND 681B, LEG 112[1]

Hedi Oberhänsli,[2] Peter Heinze,[2] Lieselotte Diester-Haass,[3] and Gerold Wefer[2]

ABSTRACT

Indicators of surface-water productivity and bottom-water oxygenation have been studied for the age interval from the latest Pleistocene to the Holocene at three holes (679D, 680B, and 681B) located in the center and at the edges of an upwelling cell at approximately 11°S on the Peruvian continental margin. Upwelling activity was maximal at this latitude during $\delta^{18}O$ Stages 1 (lower part), 3, the upper part of 5, the lower part of 6, and 7, as documented by high diatom abundance. During these time intervals, the bottom water was poorly oxygenated, as documented by low diversity benthic foraminiferal assemblages that are dominated by *B. seminuda* s.l. Both surface- and bottom-water-circulation patterns appear to have changed rapidly over short time intervals. Due to changes in surface circulation, the intensity of upwelling decreased, thereby decreasing the concentration of nutrients, and reducing the supply of organic matter to the bottom. Radiolarians became more abundant in the surface waters, and the bottom-water environment was less depleted in oxygen, allowing for the establishment of more diverse benthic foraminiferal assemblages. Surface-water productivity was probably minimal during the early part of $\delta^{18}O$ Stages 5 and 9, as indicated by the increased abundance of planktonic foraminifers and pteropods and their subsequent preservation.

INTRODUCTION

The Peruvian coastal area is located in a distinctive atmospheric and oceanic circulation regime. As a result of the southeasterly trade winds, nutrient-rich water upwells along the coast and reaches the photic zone in a belt that is approximately 10 km wide and parallels the coastline. Today, high primary production along the Peruvian coast is patchy and is concentrated in the zones of 7°–8°S, 11°–12°S, and 14°–16°S latitude. However, only from 11° to 14°S does this high fertility manifest itself in the underlying sediments (Suess et al., 1986). Within this zone, plenty of organic matter accumulates and reaches >5% (weight) of the sediment. North and south of this zone, the organic-carbon contents and sediment-accumulation rates are considerably lower despite the favorable surface-water conditions (Ingle et al., 1980; Reimers and Suess, 1983).

In a high-fertility environment the consumption of oxygen in the subsurface-water layer is enormous. The excessive supply of organic tissue to the water column rapidly depletes the oxygen downward. Today, the top of the (upper) oxygen-minimum zone of a coastal upwelling setting may be as shallow as 50 to 100 m, and the lower boundary may reach to a depth of at least 500 m (Wyrtki, 1962; Smith, 1963, 1964; Brockmann et al., 1980).

West of Peru, the main offshore flow (Peru-Chile Current: rich in oxygen and high salinity; Wyrtki, 1962; Reid, 1973) occurs in a surface layer approximately 25 m thick (Smith, 1983). According to Smith, the compensating onshore flow that feeds this upwelling is part of a poleward-directed undercurrent (Peru Countercurrent; Fig. 1). Off Peru, the poleward undercurrent is continuous from at least 5° to 15°S (Brockmann et al., 1980). The poleward flow extends from about 20 m depth over the shelf, down to a depth of 200 to 300 m on the slope. Where the current contacts the bottom, fine particles can be transported on the shelf and the slope considerable distances away from their source areas, in a direction opposite to the prevailing winds and surface currents.

For at least the last 2 to 3 Ma, several basins have rapidly subsided on the active continental margin off Peru; these basins, which include the Lima and Salaverry basins, may provide ideal conditions for high-resolution studies due to the high sedimentation rates within them. However, high subsidence rates also increase the probability that redepositional processes are active. As a consequence of such processes, an additional influx would overprint the primary, climatically (glacially/interglacially) triggered sediment-distribution pattern.

Sediments formed during upwelling events bear specific signals that, if read carefully, can be directly interpreted. Preservation of these primary signals is highly dependent on bulk sedimentation and terrigenous-influx rates, diagenesis, and physical and chemical oceanographic parameters (e.g., currents, oxygen concentrations in the water column, and bottom morphology). Bremner (1983) and Krissek and Scheidegger (1983) developed an approach for evaluating this particular type of sedimentary environment. They estimated the strength of the upwelling signature by combining various types of sedimentological data. We have applied their general concept and examined both the coarse-size fractions and benthic foraminiferal assemblages from three holes located on an east-west transect through the area of intense upwelling and well-preserved modern sedimentary indicators (Fig. 2). The time interval investigated spans the last 730 k.y.

Several studies (e.g., DeVries and Pearcy, 1982; Romine and Moore, 1981) noted that distributions of sedimentological parameters that indicate upwelling intensity are not directly linked to glacial/interglacial changes. This observation also was confirmed by our findings. Tectonic activity, which produces subsidence in the study area, as well as variations in sea level resulting from climatic changes overprint and mask primary productivity indicators.

[1] Suess, E., von Huene, R., et al., 1990. *Proc. ODP, Sci. Results*, 112: College Station, TX (Ocean Drilling Program).
[2] Universität Bremen, Geowissenschaften, D-2800 Bremen 33, Federal Republic of Germany.
[3] Universität des Saarlandes, Institut für Geographie, D-6600 Saarbrücken, Federal Republic of Germany.

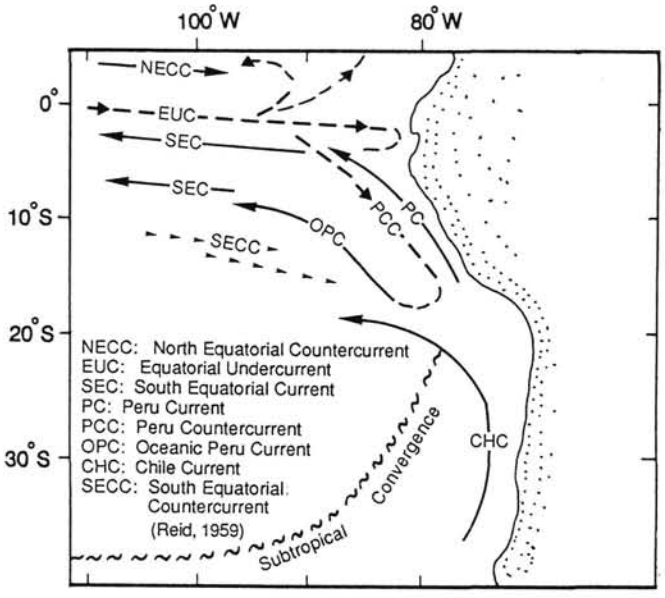

Figure 1. Surface and subsurface current patterns of the eastern Pacific Ocean (Reid, 1959; Wyrtki, 1967). Surface currents are indicated by solid lines, while subsurface currents are marked by dashed lines or arrows.

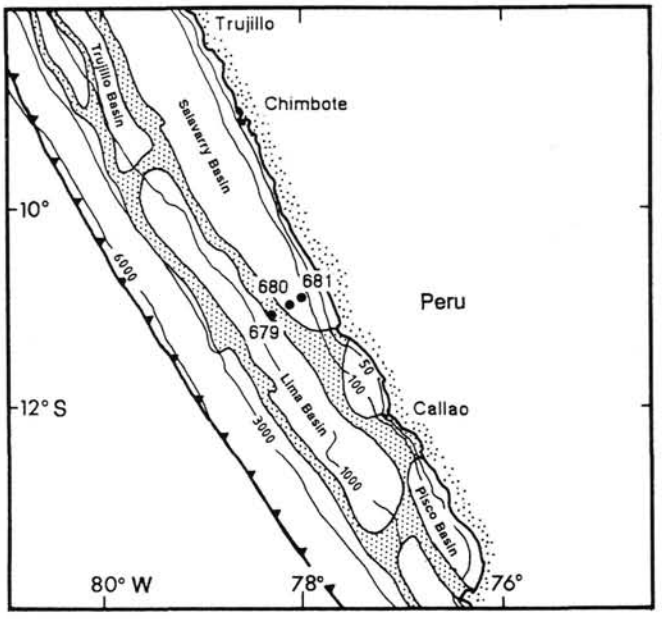

Figure 2. Location map of the studied drill sites of Leg 112: Hole 679D: 11°03.83′S, 78°16.33′W, 439.5 mbsf; 680B: 11°03.90′S, 78°04.67′W, 252.5 mbsf; Hole 681B: 10°58.60′S, 77°57.46′W, 150.5 mbsf.

Our aim was to answer the following questions:

1. How does productivity in the Peru upwelling system change over a (single) glacial/interglacial cycle?
2. Did the upwelling cell migrate in either the east-west and/or the north-south directions over these cycles?

LITHOLOGY AND STRATIGRAPHY

At Holes 679D and 680B, the Quaternary and Holocene sediments consist of laminated and bioturbated olive-gray to dark gray diatomaceous muds (Fig. 3). At Hole 680B, silty and sandy intercalations occur frequently at a depth of 15 to 35 m. At Hole 681B, the uppermost 34 m of the cored section consists mainly of dark olive-gray diatomaceous muds, with intercalated thin laminae of diatomaceous ooze. The silt content is generally high. A coarsening of the sediments at Hole 681B can be observed in several distinct intervals. These sediments are mostly laminated, although bioturbation can be observed at a depth of 12 to 15 m below seafloor (mbsf). A number of distinctly graded sandy/silty beds are present. From 34 to 47 mbsf, the silt/sand content increases sporadically and bioturbation becomes more frequent.

At Holes 679D and 680B, the Brunhes/Matuyama boundary (730 k.y.) is located at 7.63 mbsf and between 35.73 and 36.0 mbsf, respectively (Fig. 3; after Suess et al., 1988). This boundary has not yet been found at Hole 681B. At Hole 680B, oxygen-isotope data for *Bolivina* sp. (Wefer et al., this volume) allow for a more detailed chronostratigraphic resolution of the last 430 k.y. Using the age assignments for $\delta^{18}O$ Stages 1 through 11 from Imbrie et al. (1984), the topmost 30 m at Hole 680B has been dated (Fig. 3). Beyond Stage 11, the age assignments are complicated by hiatuses and reworking events. Based on the stratigraphic data available, no age assignments are possible at Hole 681B. Therefore, no stratigraphic correlations among Holes 680B, 679D, and 681B have been proposed in this study.

As displayed in the age/depth plot (Fig. 4), average sedimentation rates at Hole 680B range between 4 and 15 cm/k.y. for the last 430,000 yr. No sedimentation rate has been indicated for Stage 1 because it is not known whether the section is complete at the top. However, DeVries and Pearcy (1982) reported a Holocene sedimentation rate of 19 cm/k.y. for the shelf area off Peru, which is approximately equal to the sedimentation rate (approx. 17 cm/k.y.) observed at Hole

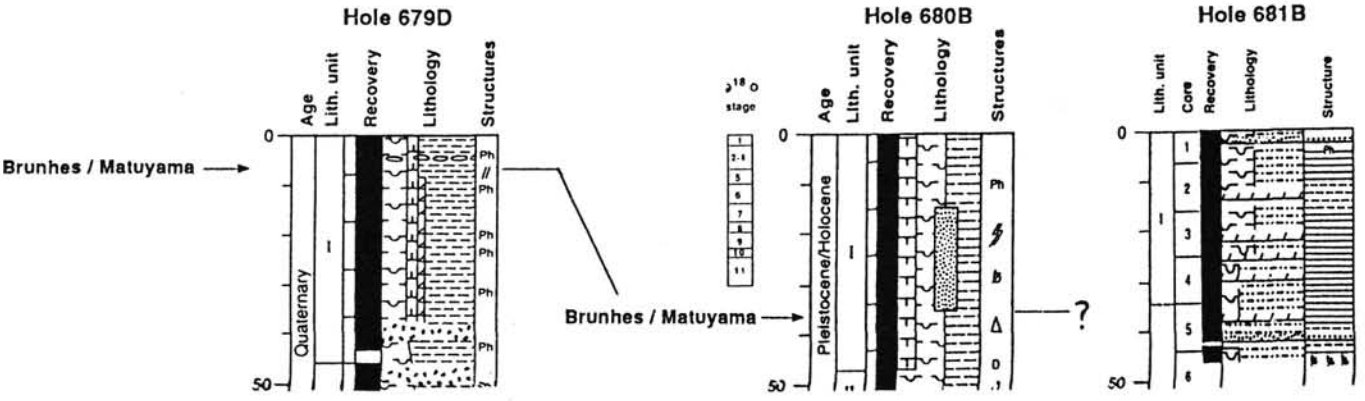

Figure 3. Lithologic columns of Holes 679D, 680B, and 681B. The Brunhes/Matuyama boundary of Holes 679D and 680B is indicated according to the site reports (this volume). Oxygen isotopic stages of Hole 680B are based on Wefer et al. (this volume).

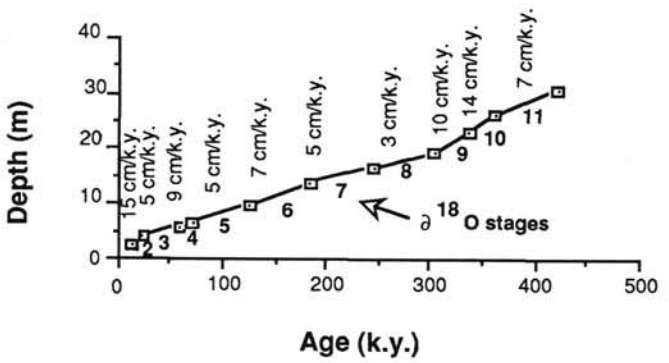

Figure 4. Age-depth plot of Hole 680B, based on the oxygen-isotope values reported in Wefer et al. (this volume). Numbers indicated beneath the curve relate to the $\delta^{18}O$ stages. In addition, the sedimentation rates for Stages 2 to 11 are indicated and are based on stage-boundary age assignments given by Imbrie et al. (1984).

680B, if the Holocene section is assumed to be complete. The sedimentation rates calculated for Hole 680B are about an order of magnitude lower than the sedimentation rates reported by Reimers and Suess (1983) for upper-slope sediments off Peru at 11°15'S and 15°09'S. These authors observed average sedimentation rates ranging between 30 and 120 cm/k.y. for the last 15,000 yr.

MATERIALS AND METHODS

Samples from Holes 679D, 680B, and 681B (which form a transect across a portion of the continental margin, perpendicular to the coast of Peru; Fig. 2), were selected for this study. Holes 679D and 680B provide information about the sedimentary environments on the outer and inner flanks of the ridge situated between the Lima and Salaverry basins. Hole 681B is located in the central part of the Salaverry Basin.

For all holes, weight percentages of the clay/silt fractions (<63 μm) were measured by wet-sieving (P. Heinze). These data are listed in Appendixes 1 and 2.

At Hole 680B, the >63-μm fraction was analyzed qualitatively and quantitatively (P. Heinze; after the method developed by Sarnthein, 1971). The coarse-fraction analysis is based on visual percentage estimates. The percentage of the planktonic and benthic foraminifers, radiolarians, diatoms, fish remains, and phosphorites were calculated on a terrigenous-free basis to obliterate the allochthonous contribution that might mask the primary autochthonous signal. All curves of these components have been smoothed by five-point (1-4-6-4-1), running-weighted average procedure. Uncorrected data of these components, including the terrigenous constituents, are reported in Appendix 1. In addition, the quantitative composition of the samples was calculated on an aggregate-free basis. Aggregate probably formed often because of the partially high organic-carbon content, although the sediments were wet-sieved.

To provide more detailed data for Hole 680B, the sedimentary petrography of the >40-μm size fraction of samples from Core 112-680B-2H (interval 112-680B-2H-1, 3 cm, to 112-680B-2H-7, 16 cm) was analyzed (L. Diester-Haass). Approximately 800 grains of each size fraction (40–63 μm, 63–125 μm, 125–500 μm, >500 μm) were counted.

At Holes 679D and 681B, the abundances of terrigenous constituents (mainly quartz, feldspars, and mica), biogenic opaline components (diatoms and radiolarians), and fish remains were generally estimated using the categories none, few (1%–25%), common (25%–50%), and abundant (>50%) (H. Oberhänsli). Accumulation rates for planktonic and benthic foraminifers, diatoms, radiolarians, and terrigenous contents were calculated only for the interval Core 112-680B-2H because density data are sparse (7 random values for 33 m core material).

Table 1. List of benthic foraminifer genera and species identified.

Bolivina alata (Brady)
Bolivina costata d'Orbidny
Bolivina interjuncta bicostata Cushman
Bolivina minuta Natland
Bolivina plicata d'Orbigny
Bolivina salvadorensis Smith
Bolivina seminuda s.l. Cushman
Bolivina sinuata Galloway and Wisler
Bolivinia spissa (Cushman)
Bolivina subfusiformis Cushman
Bulimina denudata Cushman and Parker
Bulimina elegantissima (d'Orbigny)
Bulimina marginata d'Orbigny
Buliminella curta Cushman
Cancris auricula (Fichtel und Moll)
Cassidulina cushmani Stewart and Stewart
Cassidulina subglobosa Brady
Cassidulina limbata Cushman and Hughes
Cassidulina tumida Natland
Epistominella bradyana (Cushman)
Epistominella exigua (Brady)
Epistominella obesa Bandy and Arnal
Epistominella pacifica (Cushman)
Globobulimina sp.
Gyroidinoides altiformis Stewart and Stewart
Gyroidinoides rothwelli Natland
Nonionella auris Cushman
Nonionella stella Cushman and Moyer
Planulina ornata d'Orbigny
Pullenia sp.
Stainforthia sp.
Suggrunda eckisi Natland
Textularia sp.
Trifarina angulosa (Williamson)
Trifarina carinata (Cushman)
Uvigerina peregrina s.l. Cushman
Valvulineria inflata (d'Orbigny)
Virgulina spp.
Virgulinella spp.

Parallel to the sedimentological studies, benthic foraminiferal assemblages from selected intervals of Holes 679D (H. Oberhänsli), 680B, and 681B (P. Heinze) were qualitatively and quantitatively analyzed. Samples were divided with a microsplitter until 200 to 600 specimens remained in the tray. On average, a minimum of 300 specimens was counted in the >125-μm size fraction at Holes 680B and 681B and in the >63-μm fraction at Hole 679D (Table 1; Appendixes 3 through 5).

RESULTS

To trace and estimate the extent of changes in paleoproductivity and sea level in response to glacial and interglacial climate, we report qualitative and quantitative analyses of the abundance of biogenic opaline components, biogenic calcareous fragments, phosphorite, fish remains, planktonic and benthic foraminifers (calculated on a terrigenous-free base), and the terrigenous constituents. In addition, we use the organic carbon and carbonate measurements (Suess et al., this volume) to monitor environmental changes.

Hole 679D

Hole 679D is located at the outer edge of the high productivity zone at 11°S. The typical high productivity indicators, such as diatoms, are dominant components only in a few of the 15 studied samples (Fig. 5). The semiquantitative analyses of the >63-μm size fraction show maxima of fish remains in the topmost 0.5, 2.73, and 3.73 mbsf. Phosphorites occur as minor constituents at 2.73, 4.23, and from 5.73 to 6.25 mbsf.

Radiolarians reach their maximum abundance above 2 and shortly below 2 mbsf. Planktonic foraminifers show highest

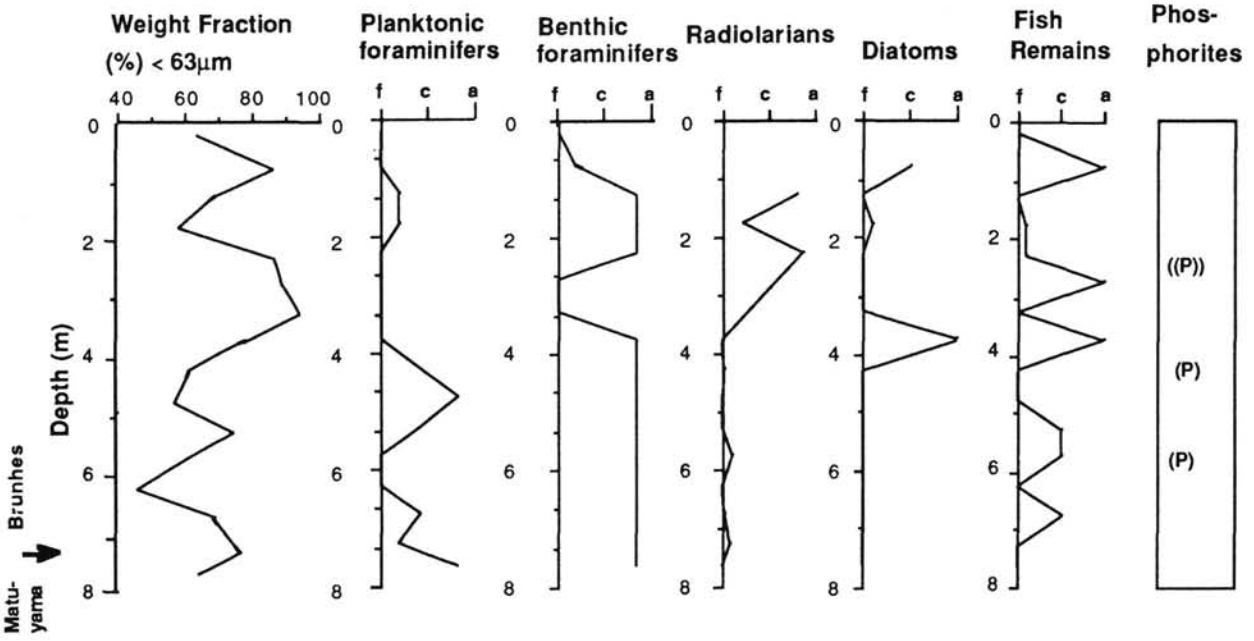

Figure 5. Weight percentages of the <63-µm size fraction, radiolarians, planktonic foraminifers and benthic foraminifers, as well as semiquantitative estimates of diatom, fish remains, and phosphorite abundances at Hole 679D (f = few, c = common, a = abundant).

concentrations at 2, 4.73, and 7.23 mbsf. Benthic foraminifers are abundant in most studied samples.

According to the stratigraphic distribution of abundances of individual species, the benthic foraminiferal assemblages can be divided into six groups (A through F; Fig. 6). The groups resulting from visually fitting the abundance curves of different species are considered to represent the environmental evolution of the bottom water over the time slice investigated. The lower part of the section is governed by Groups A through D, while the upper part is dominated by Groups E and F.

Hole 680B

The data set from Hole 680B has been organized as follows: Figures 7 and 8 document the sedimentary evolution of the last 730 k.y.; Figures 9 and 10 display a more detailed view of the time slice at about 200 to 60 k.y. ago. This interval spans the top of $\delta^{18}O$ Stage 7 to the lower part of Stage 4. The 730-k.y. record contains the analyses of the >63-µm size fraction, whereas the 200- to 60-k.y. record is based on sample material >40 µm.

Hole 680B is located in the center of the coastal upwelling zone at 11°S. This hole is promising with regard to our aims because precise ages can be assigned to the topmost 30 m of the sedimentary record (Figs. 4, 7, and 8). However, the carbonate and organic-carbon contents (Fig. 7, from Suess et al., this volume), as well as the abundance of terrigenous constituents in the >63-µm size fraction (Fig. 7), do not exhibit cyclic changes that can be directly related to glacial/interglacial changes. The carbonate content is low (<10%) in Stages 1, 6, and 7 and in the upper parts of Stages 2 through 4, and 10. Intermediate values (15%–25%) occur episodically within Stages 3 through 5 and throughout Stages 7 through 9. In Stages 10 (bottom) to 11, carbonate values range from 25% to 60%. The organic-carbon content is low for an upwelling environment (<5%) in the upper part of Stages 2 through 4, at the Stage 5/6 transition, and in Stages 10 and 11. The level of organic carbon is higher (>5%), with several exceptions, during Stages 1, 2 through 4, the upper parts of 5 and 6, 7 through 9, and 11. A comparison of the organic-carbon contents with terrigenous contents shows that minima in the organic-carbon contents coincide with increased terrigenous abundance, except for lower Stage 5 (Fig. 7). The terrigenous abundance is relatively low (<10%) in Stages 1 and 3(?) through 6, although a few samples with increased detrital abundance (20%–30%) were observed in these intervals. In the uppermost part of Stages 2 through 4, the terrigenous content increases considerably and reaches 30%. From Stage 7 down to the Brunhes/Matuyama boundary, detrital abundances are highly variable (5% to 50%).

Results of the quantitative component-abundances in the >63-µm fraction are shown as smoothed curves in Figure 8 to select major cycles. Planktonic foraminifers show maximum abundances at the lowermost interglacial event in Stages 5 (50%) and 9 (20%). The benthic foraminifers show three cycles of increased abundances (up to 80%–95%): from Stages 2 through 4 to mid-6, lower 7 to upper 9, and mid-10 to 11. Radiolarians show maximum concentrations during Stage 1, the uppermost part of Stages 2 through 4, the middle part of Stage 6, in the upper part of Stage 7 and the lower part of Stage 9, and at the top of Stage 10. Diatoms are abundant or common within Stages 1, 2 through 4 (3?), 5, in the lowermost part of 6, at the bottom and top of Stage 7, and in Stage 10. The percentages of fish remains, which are probably 7overestimated, show maxima at the top of Stages 1 and 2 through 4, Stage 6, within Stage 7, and in the lower part of Stages 9 and 11. The qualitative and quantitative compositions of the benthic foraminiferal assemblage are shown in Figure 9.

Valuable information about the major changes that accompany a transition from a glacial to an interglacial period can be gained by looking in detail at part of the entire time studied (approximately 730 k.y.). This close-up spans the time interval from about 60 to 200 k.y. ago. From Figures 10 and 11, however, the climatic break comparing glacial Stage 6 with interglacial Stage 5 and its effect on the distribution of the different sedimentary components is not evident at first glance. With the exception of diatoms and terrigenous components (which seem to be slightly higher in Stage 6 than in Stage 5), no other systematic change can be observed. Even these changes are not truly cyclic and thus are not obviously in response to climatic changes. However, a prominent event

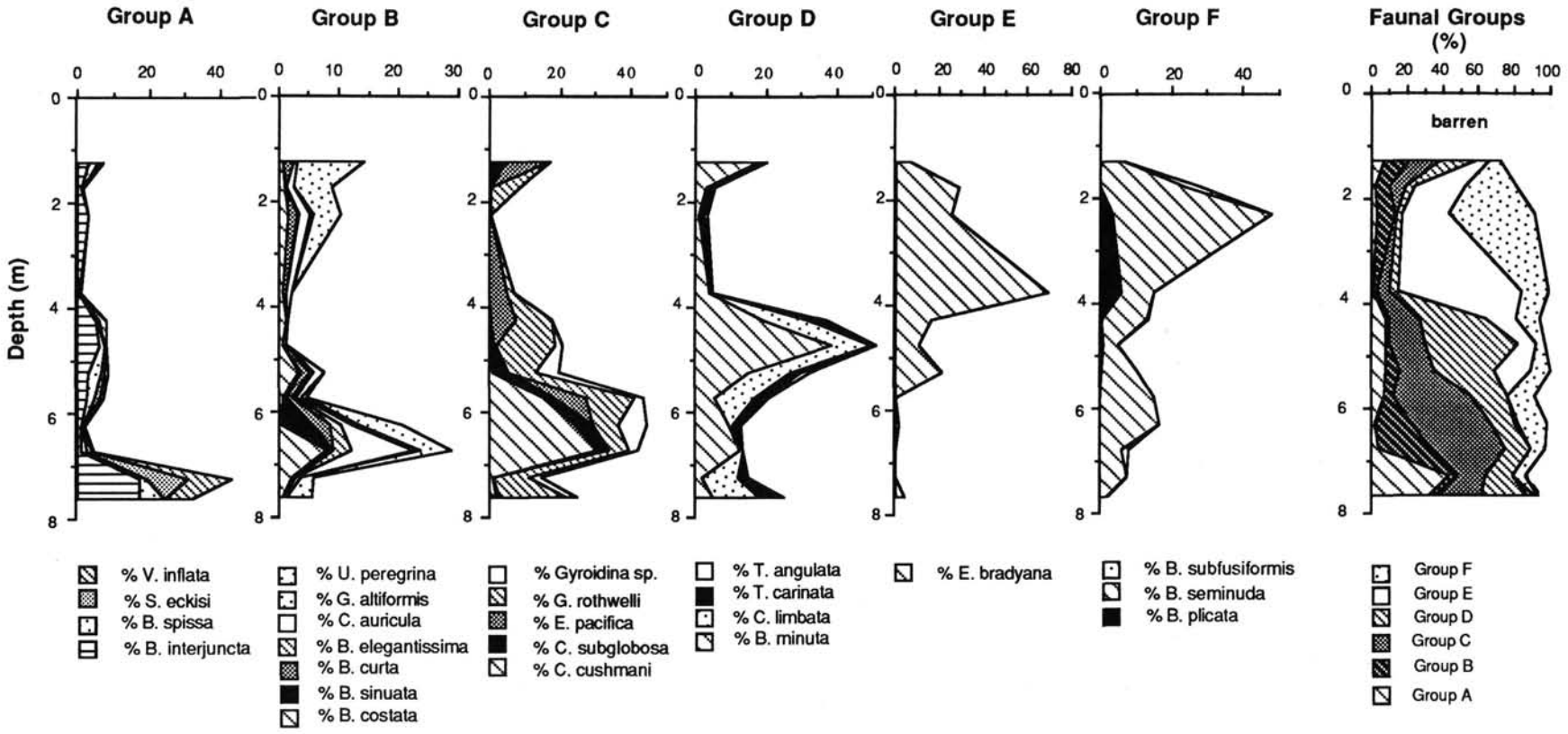

Figure 6. Benthic foraminiferal distribution pattern of selected Groups A through F at Hole 679D for the last 730,000 yr. At the left side, a composite diagram of Groups A through F is shown. The distribution pattern is determined by (1) bathymetric changes and reworking events and (2) bottom-water oxygenations (Groups A to F; see "Discussion" section, this chapter).

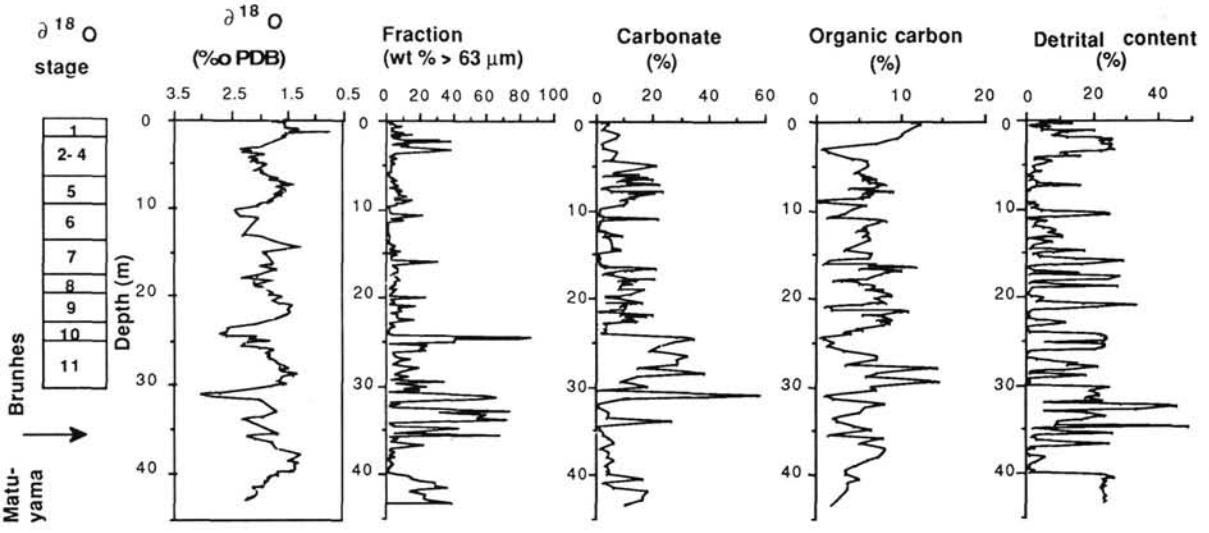

Figure 7. Weight percentages of the >63-μm size fraction, organic carbon, and carbonate (for both, see Suess et al., this volume), as well as detrital content at Hole 680B. For the temporal relationship, the $\delta^{18}O$ record (Wefer et al., this volume) and the Brunhes/Matuyama boundary (see various site reports, Suess, von Huene, et al., 1988) are shown.

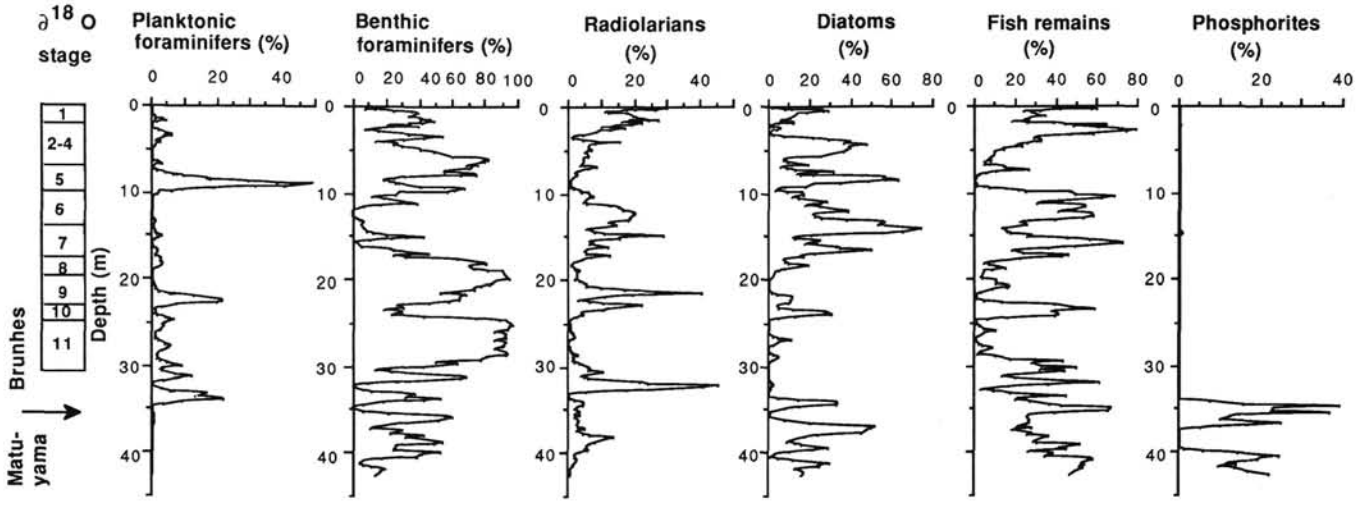

Figure 8. Analyses of the >63-μm size fraction from Hole 680B. The percentages of the planktonic and benthic foraminifers, radiolarians, diatoms, fish remains, and phosphorites are calculated on a terrigenous-free basis. All curves are smoothed by a five-point, running-weighted (1-2-5-2-1) average procedure. In addition, the quantitative composition of the samples was calculated on an aggregate-free basis.

is documented by the calcareous organisms near the Stage 5/6 transition. Between 8.8 and 9.2 mbsf, which is equivalent to the lower part of Stage 5, the planktonic foraminifers, pteropods, and gastropods each reach maximum abundances (Fig. 11). Coincident with these maxima, the abundances of *B. seminuda*, organic carbon, benthic foraminifers, and diatoms decrease significantly. Terrigenous content, fish remains, and radiolarians are also low during this time interval (Figs. 9, 10, and 11).

Hole 681B

At Hole 681B, several distinct and short-lived reworking events are documented by the detrital distribution (Fig. 12). Diatom abundance is maximal at 2–3, 6–10, 20, and 22 mbsf. Radiolarian presence at 4–6 and 10–12 mbsf coincide mostly with diatom minima. The distribution of fish remains, which is generally correlated negatively to diatom abundance, shows maxima between 3 and 5 mbsf and at 18 mbsf. Planktonic foraminifers, although generally rather sparse, are abundant at 1.73 mbsf (Fig. 12). A low diversity was recorded for the benthic foraminiferal assemblage; this consists mainly of *Bolivina costata*, *Bolivina seminuda*, *Nonionella auris*, and scattered *Epistominella bradyana* (Fig. 13). These four species form more than 80% of the total assemblage.

DISCUSSION

The main features of the coarse grain-size distribution that must be considered are (1) lack of a regular cyclicity in the abundance of the various components that can be related to glacial/interglacial effects in the abundance of the various components, (2) the preservation spike of planktonic foraminifers and mollusks observed in Stages 5 and 9, and (3) the benthic foraminiferal distribution pattern.

Terrigenous Influx: Changes in Sea Level vs. Tectonics

In a shallow-water environment, changes in sea level during the last 730 k.y. are of particular interest. Glacio-eustatic lowering of sea level would have had serious consequences on at least the shallowest hole studied (681B); today

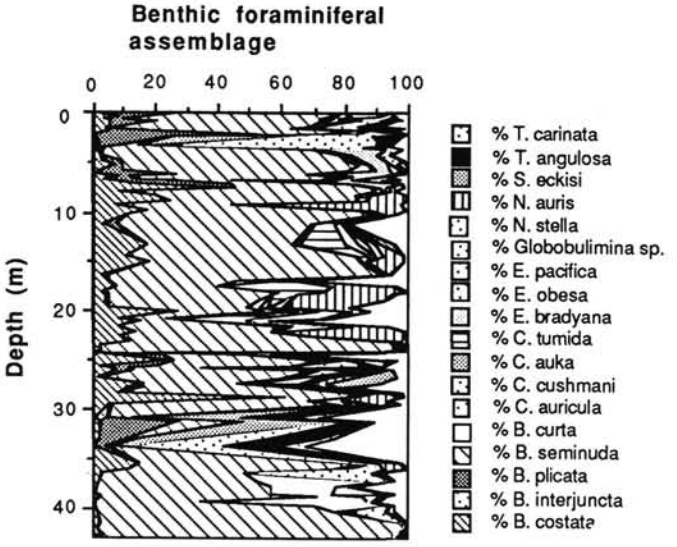

Figure 9. Composite diagram of the benthic foraminiferal composition at Hole 680B.

this hole is located at a water depth of 150 m. However, we do not know whether the expected large-amplitude changes in sea level obliterated upwelling signals at Hole 681B because we do not have a chronostratigraphic control. A lowering of sea level by 100 to 120 m during an entire glacial interval (as could be deduced from the oxygen-isotope records; Shackleton, 1977; Chappell and Shackleton, 1986), would result in considerable encroachment of the coastline toward the holes studied here. Consequently, terrigenous influx most likely has changed. Accumulation rates of terrigenous matter in Hole 680B clearly show a reduction by a factor of two from the glacial Stage 6 to the interglacial Stage 5 (1.42 to 0.63 g/cm^2 k.y.; Fig. 14). For that particular time, increased erosion at the nearby coastal area is probably responsible for this observation. However, the distribution pattern of the terrigenous constituents in Figure 7, which depicts the entire interval studied at Hole 680B, is more random. Factors other than changes in sea level may have controlled the detrital influx.

Further, bottom currents may be important for the distribution pattern of detritus. The positive correlation between some detrital spikes and abundances of phosphorites and fish remains (Figs. 7, 8, and 12) indicates increased bottom-current activities, which probably are linked to changes in sea level. According to Bremner (1983), phosphorites, and fish bones to a large extent, are mostly present as lag deposits, which represent increased winnowing. Therefore, the presence of these components in combination with higher detrital contents may indicate time intervals of higher bottom-current activity.

In addition to modifications of the bottom-current regime and sea-level-induced changes (the latter possibly producing muddy flood events; Quinn et al., 1978), tectonics may account for the random occurrence of allochthonous components in both glacial and interglacial intervals. On the active continental margin off Peru, the pre-Quaternary subsidence rate locally was considerable (500 m/m.y.; Kulm et al., 1981) and resulted in redepositional events. Slumps, slides, and turbidites are common features in the upper Miocene and Pliocene sedimentary record of the Lima Forearc Basin (e.g., Holes 682, 679; see von Huene et al., this volume). Hole 679D lies slightly beyond the edge of the shelf, so that slump-produced hiatuses may be relatively common, and the completeness of the sequence is questionable. At Holes 680B and 681B, tectonic origin can be assumed for several of the detrital events, particularly those documented below 30 and 35 mbsf, respectively (Figs. 7 and 12).

Several benthic species at Hole 680B (shown in Fig. 15) reveal a good correlation to the terrigenous content. Some of these individuals may represent transported and redeposited specimens. However, most of these specimens were probably coping well with the prevailing silty/sandy substrate and thus may be autochthonous (Resig, this volume). These specimens survived because of the sandy/silty substrate, to which they were better adapted and probably also survived because of currents supplying oxygen-enriched water to the poorly oxygenated bottom environment (e.g., Lutze, 1962, 1964; Quintero and Gardner, 1987; Resig, this volume). The faunal pattern observed at Hole 679D indicates that Groups A through D represent bottom-water conditions either sufficiently oxygenated due to currents (Groups A, C, and D) or redepositional events (Group B). According to Resig (this volume), most species of Groups A, C, and D indicate an upper bathyal depositional setting for the lower part of Hole 679D.

In conclusion, the terrigenous abundances reflect three different factors: (1) varying dilution by calcareous and opaline skeletons due to fertility changes in the surface water, (2) effects of changes in sea level possibly tied to changes in the bottom-current regime, and (3) tectonics.

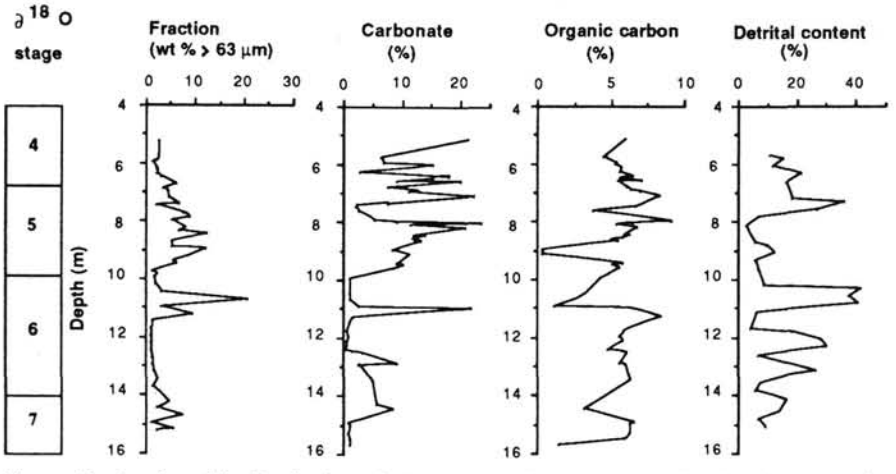

Figure 10. Stratigraphic distribution of abundances of the >63-μm size fraction, organic carbon, carbonate (Suess et al., this volume), and detrital contents (>40 μm) from a close-up of Hole 680B representing the age interval, 60,000 to 200,000 yr ago.

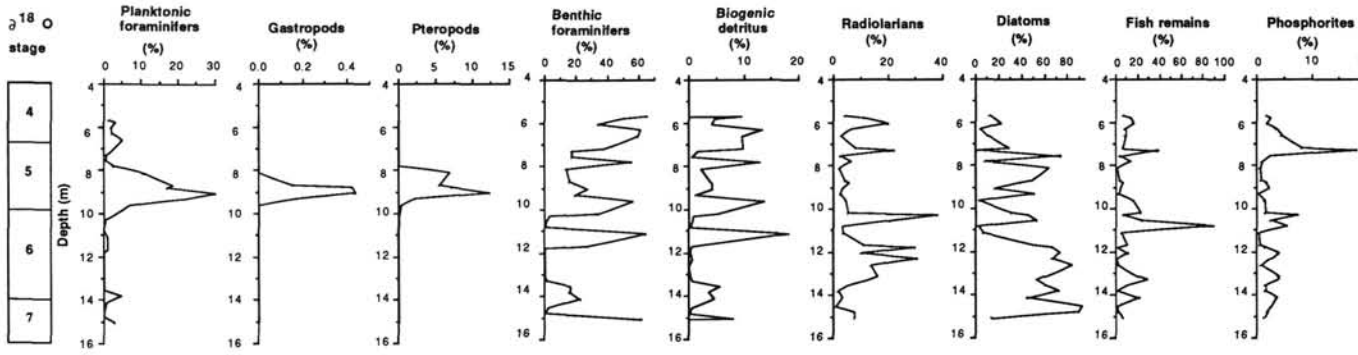

Figure 11. Composition of the >40-μm size fraction for a close-up of Hole 680B representing the age interval 60,000 to 200,000 yr ago.

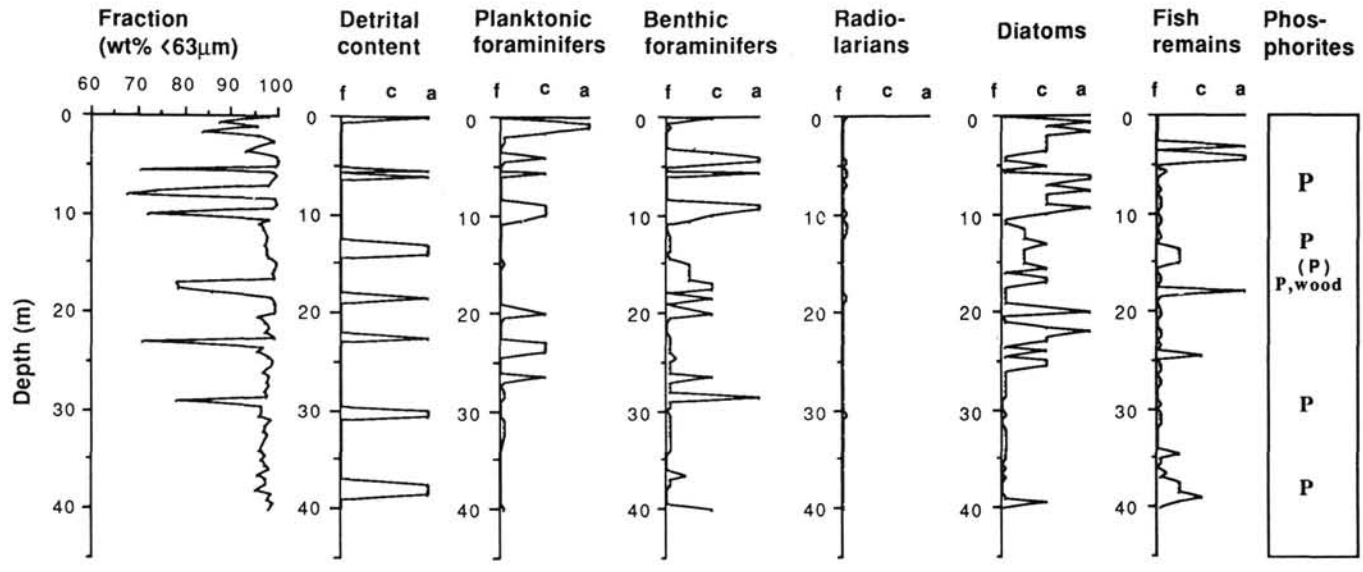

Figure 12. Abundance of the <63-μm size fraction and estimates of benthic foraminifers, planktonic foraminifers, detritus, diatoms, and phosphorite contents (f = few, c = common, a = abundant) at Hole 681B.

At present the faunal distribution pattern of selected benthic foraminifers does not indicate unequivocally which peaks of terrigenous constituents originated from tectonically induced reworking events and which were caused by intensified currents produced by glacio-eustatic changes in sea level.

Surface Currents and Paleoproductivity

Both radiolarians and diatoms are good tracers of oceanographic conditions in the surface-water mass. Diatoms dominate (phyto)plankton communities in high fertility areas (e.g., Hart and Currie, 1960; Calvert, 1966), whereas most radiolarians exhibit maximum occurrences in areas surrounding these high fertility zones (Molina-Cruz, 1984). Thus, these two components of the coarse-size fraction are good tracers of changes in the pattern of surface current. A comparison of the radiolarian and diatom distributions with abundance patterns at Hole 680B (Fig. 8) reveals an evident negative correlation, which indicates that surface-current activities changed sporadically at the area studied. The oceanographic regime in the area of interest is dominated by the Peru Current and the Peru Countercurrent (Fig. 1; Wyrtki, 1967). During intense upwelling, the advection of the Peru Countercurrent is greatly inhibited. When the southeasterly trade winds diminish, and consequently the upwelling activities of the Peru Current weaken, the Equatorial water mass surfaces and feeds the Peru Countercurrent (Wyrtki, 1967; Molina-Cruz, 1977). This scenario, which proposes a decrease in upwelling activities in the study area during those intervals when radiolarian maxima were observed, may have occurred several times during at least the last 300 k.y. Thus, based on the radiolarian abundances, periods of weakened upwelling may be documented within Stages 1, the upper part of 2 through 4, the middle part of 6, within the upper part of 7, and in Stage 9 (Figs. 8, 11, and 16).

Diatom abundances and organic-carbon contents, combined with carbonate preservation (in intermediate and shallow-water depth localities) and indicators of the degree of oxygenation of the bottom-water environment (e.g., benthic foraminiferal assemblages), are excellent tools for directly or indirectly estimating biological fertility in surface waters (e.g., Müller and Suess, 1979). However, local bottom currents and early diagenesis partly inhibit the preservation of the autochthonous sedimentary record. Favorable conditions for a complete sedimentary record of the biogenic opal may have prevailed for at least the last 300 k.y. at Hole 680B (Figs. 8 and 16). The reduced abundance or absence of diatoms below 20 mbsf (most probably due to diagenetic loss), removes relevant information for the time slice from 300,000 to 730,000 yr. ago. Averages of the diatom flux rates over the entire interval cannot be investigated at this time because of insufficient density data. Only for the time slice from 60,000 to 200,000 yr. could the accumulation rates for the diatoms be calculated (Fig. 14). The diatom flux shows no striking differences between glacial and interglacial periods. At the Stage 5/Stage 6 boundary, no significant break was observed. Average

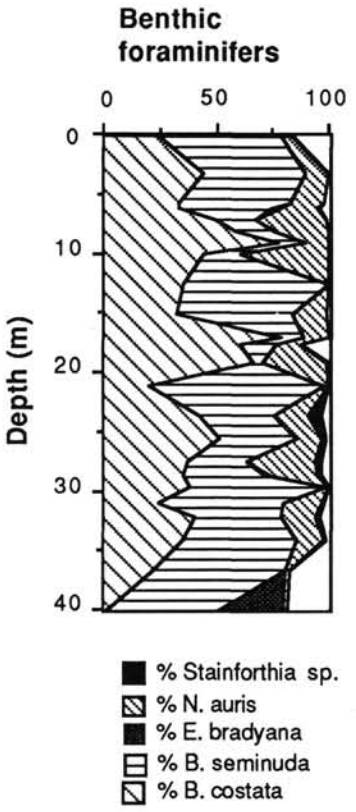

Figure 13. Composite diagram of the benthic foraminiferal composition at Hole 681B.

accumulation rates for diatoms in Stages 5 and 6 are 2.7 and 2.5 g/cm^2 k.y., respectively, indicating similar rates for glacial and interglacial periods. This trend observed for the glacial/interglacial cycles representing Stages 6 and 5 seems to contrast with rates observed by Müller and Suess (1979), who pointed out that upwelling intensity off West Africa was strongest not during the last glacial maximum (18,000 yr.), but during Stage 3 and for a short period during early Stage 1. At present, we think that the sparse density data at Hole 680B do not allow us to reconstruct the flux rates properly. We postulate that on the basis of the diatom distribution pattern at Hole 680B, upwelling intensity was strongest at this location during Stages 1, 2 through 4 (the maximum is probably centered within Stage 3), the upper parts of 5 and 7, and through 6 and 10(?) (Fig. 16; see also Schrader, this volume). This data matches too strongly with the organic-carbon contents, which show coevally maximum values although the organic carbon contents exhibit more flat-topped broad peaks and not so much variability.

The calcareous preservation maxima, as documented by the increased abundance of planktonic foraminifers, are located in Stages 5 and 9 (Fig. 8). However, the quality of the carbonate preservation is different. In Stage 5, abundant planktonic foraminifers, pteropods, and benthic mollusks have been preserved (Fig. 10). This indicates that the concentration of carbon dioxide in the water column had reached a minimum level because of lowered decay rates of organic tissue. The abundances of diatom and organic carbon are low within this time interval, indicating that upwelling activity briefly decreased considerably or stopped during periods when the preservation of calcareous organisms was excellent. Similarly, Sarnthein et al. (1982) reported a preservation spike from the eastern Equatorial Atlantic during early Stage 1 that they attributed to reduced coastal upwelling.

However, on the basis of the abundance pattern of calcareous planktonics observed at Hole 680B, upwelling activity was probably reduced more drastically during Stage 5 than Stage 9.

Changes in Bottom-Water Environment in Relation to Surface-Water Productivity

Changes in bottom-water environment, which are thought equally to mirror the global climatic evolution, are documented by benthic foraminiferal abundances and the relative proportions of selected benthic species. Fragmentation rates of calcareous fossils may provide information about the dissolution potential of the bottom water, whereas the distribution of size fraction (in combination with terrigenous constituents) may help to trace bottom-current activities.

Benthic foraminiferal genera and species have different preferences with respect to their habitat (for the Peru-Chile coastal area see the following papers: e.g., Bandy and Rodolfo, 1964; Resig, 1976; Ingle et al., 1980). Factors that have most likely varied in the study area over the last 730,000 yr. are (1) water depth, (2) substrate type and water clarity (see discussion in previous sections), and (3) the availability of nutrients and oxygen.

The holes studied are located today at the shelf edge (680B and 681B) and on the upper slope (679D, upper bathyal depth). Glacio-

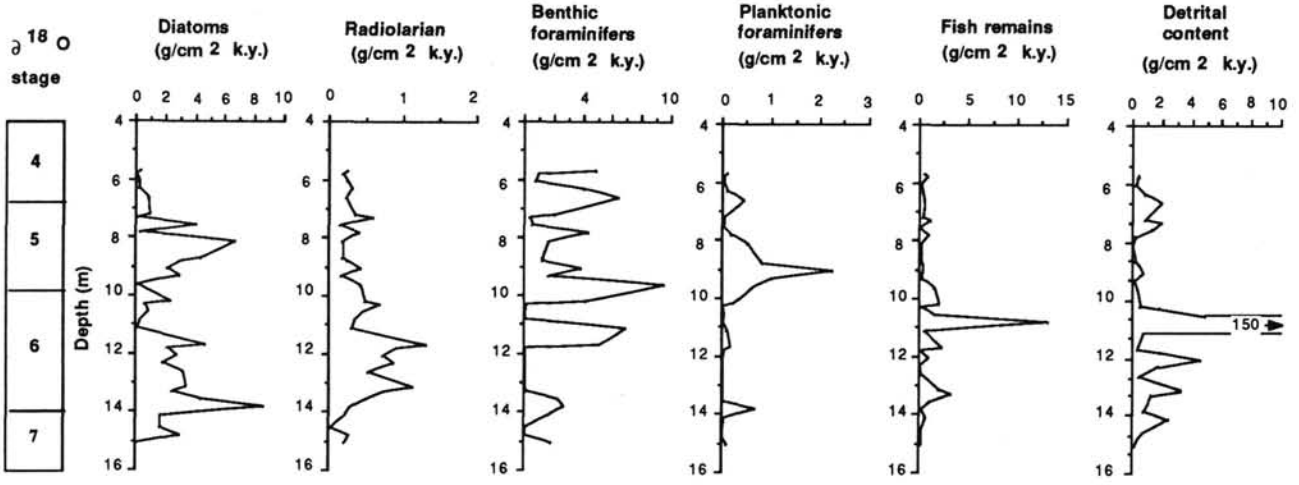

Figure 14. Accumulation rates for selected components of Stage 4 through the upper part of Stage 7 at Hole 680B.

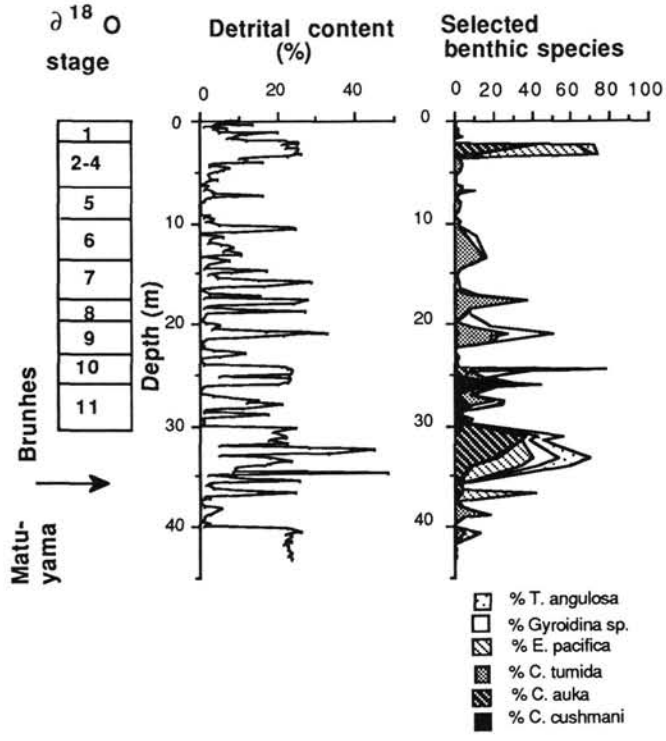

Figure 15. Distribution of selected benthic foraminifers, indicating both mass transport and winnowing events and/or better bottom-water oxygenation at Hole 680B.

eustatic changes in sea level probably reduced water depth by several tens of meters during glaciation, but the fluctuations in water depth may have been modified by subsidence.

In the high-fertility center of the area of the holes studied, the availability of nutrients and oxygen was crucial for the evolution of the bottom-water environment. In most intervals nutrients were always available in excess (see organic-carbon content in Fig. 7) in the sediment/water interface. Thus, in most intervals it was mainly oxygenation of the bottom water that influenced the benthic foraminiferal assemblages. The oxygen content in the bottom water depends on two factors: (1) fertility in surface water and (2) current systems. The availability of oxygen in the bottom water can be traced by the abundance of *Bolivina seminuda* s.l., *Globobulimina* sp., *Bolivina costata* and *Nonionella auris* because these species react very sensitively to the oxygenation state of the habitat. According to Phleger and Soutar (1973), *B. seminuda* s.l. tolerates concentrations of oxygen far less than 0.5 mL/dm^3. The distribution pattern of *B. seminuda* s.l. at Holes 679D, 680B, and 681B (Figs. 17 to 20) shows that a maximum average abundance was reached at Hole 680B. This may indicate that this location was situated most of the time in the oxygen-minimum layer.

The abundance pattern of *B. seminuda* s.l. reveals many fluctuations, showing values as high as 90%. These intervals indicate oxygen-minimum conditions at Hole 680B (Figs. 16, 17, 18). We assume that the position of the oxygen-minimum zone is indicated by the intervals where the abundance of *B. seminuda* exceeds 50%. This value may be somewhat arbitrary. However, it is based on several observations. Today, abundances of B. *seminuda* reach 60% in the center of the upwelling zone at Hole 680B (Fig. 17), where bottom-water oxygenation may be as low as 0.2 mL/dm^3 (Reimers and Suess, 1983). A slight rise in the concentration of oxygen (by 0.1 to 0.2 mL/dm^3) in the oxygen-minimum zone may lower the abundance of *B. seminuda* by 5% to 10%. Therefore, a 50% abundance of *B. seminuda* documents a threshold value because it often coincides with significant abundance changes (e.g., surpassing the average values) of *Globobulimina* sp., *B. costata* and *N. auris*. During the last 150,000 yr. the fluctuations of the abundance of *B. seminuda* represent times of increased surface-water fertility, combined with limited bottom-water circulation at the site studied (Fig. 16). The maximum occurrences of this benthic species coincide mostly with peaks in the abundance pattern of diatoms at Hole 680B, except for Stage 6 (we observed a slight time lag) and for those time intervals (Stage 11) when diagenetic alteration destroyed the primary biogenic opal record (Fig. 8, 10, and 11).

Abundance peaks of *Globobulimina* sp. precede or follow the maximum abundance of *B. seminuda* s.l. This species is present at Holes 679D (located in an upper bathyal setting throughout the Quaternary age; Resig, this volume) and 680B, but is missing completely at Hole 681B (Figs. 17 to 20). From its observed temporally and spatially limited distribution pattern, we conclude that *Globobulimina* sp. need slightly better oxygenation than *B. seminuda* s.l. and are most probably restricted to the water layer below the oxygen-minimum zone.

The distribution of *B. costat*a at Holes 680B and 681B correlates negatively with the abundance of *B. seminuda* s.l. (Figs. 17 through 19). *B. costata*, when compared with Hole 680B, shows higher concentrations throughout the shallow Hole 681B. This abundance pattern indicates that bathymetry also may be a factor that influences the occurrence of this species (Resig, this volume). At Hole 679D, *B. costata* is restricted to the lower part of the studied section (Fig. 6, faunal Group B), probably indicating reworking events of shallower sediments. We may draw the following conclusions:

1. *B. costata* prospered when the concentration of oxygen improved, probably reaching an oxygen content of 0.5 to 1 mL/dm^3.
2. The spatially restricted distribution, as well as the abundance pattern, may indicate that *B. costata* is restricted to the layer above the oxygen-minimum zone.

The maximum abundance of *N. auris* can be observed at Holes 681B and 680B (Figs. 17 to 19). Its maxima always preceded the maximum percentage of *B. costata*. In Core 112-680B-2H (Fig. 17), the *N. auris* maximum coincided with the preservation spikes of planktonic calcareous shells. We may conclude that *N. auris* indicates even better oxygenated bottom waters than *B. costata*.

Therefore, the distribution patterns of *N. auris*, *B. costata*, *B. costata*, and *Globobulimina* sp. at the holes studied can be used to explain fluctuations in oxygen concentrations in bottom waters. From the temporal succession of *B. seminuda*, *B. costata*, *N. auris*, and *Globobulimina* sp. recorded in Figures 17 through 20, we have traced spatial displacements of the oxygen-minimum zone mainly at Hole 680B, because a chronostratigraphic control on the environmental changes in bottom water exists only for this hole (Figs. 16 and 17). Other environmental modifications, such as the expansion or shrinking of the oxygen-minimum zone due to an intensified upwelling or lateral shifts of the upwelling cell, cannot be established until a better chronostratigraphic control for Holes 679D and 681B is available.

At Hole 680B (Fig. 18), a *B. seminuda* s.l. maximum in Stage 6 is followed by the abundance maximum of *N. auris* at the bottom of Stage 5. This faunal change documents a drastic improvement in bottom-water oxygenation. At the same time, surface-water productivity changed drastically. While high fertility-indicating diatoms reached a minimum at that time, calcareous plankton reached a maximum coevally. The latter

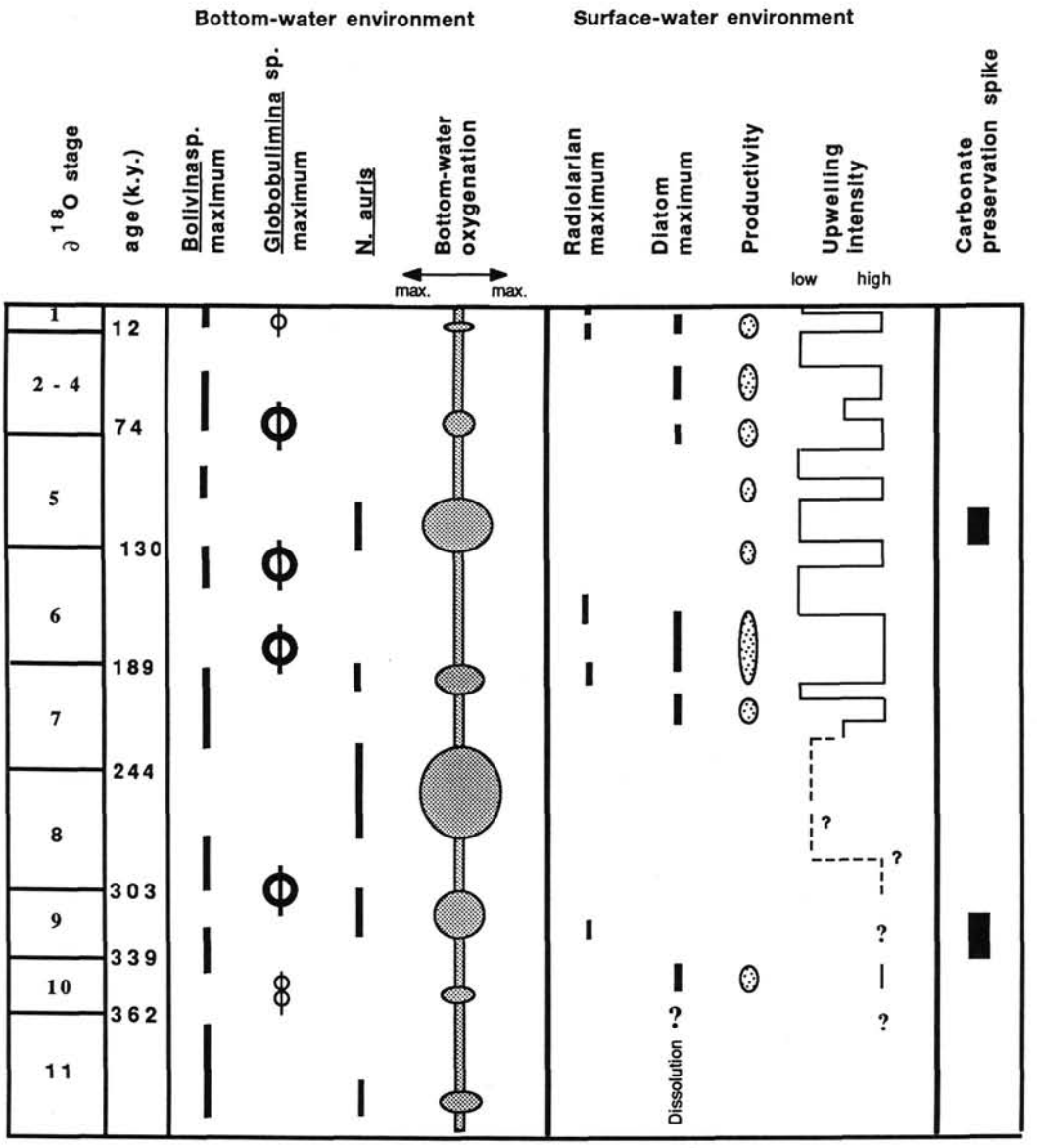

Figure 16. Sketch of environmental changes at Hole 680B over the last 423,000 yr, as deduced from selected components. These changes were interpreted to reconstruct an upwelling history for the respective time interval. A sequence of bottom current and fertility changes is also proposed.

are well preserved (Figs. 11 and 16). Bottom currents also were more intense during this time interval as indicated by the *N. auris* maximum. The maximum abundance of *B. costata*, which was recorded after the *N. auris* maximum and was itself followed by a *Globobulimina* sp. peak, indicates that bottom-water oxygen levels progressively decreased (Fig. 18). This probably resulted from a steady reestablishment of increased surface-water fertility.

A scenario similar to that for Stage 5 at Hole 680B can be proposed for the succession of *N. auris*, *B. costata*, and *B. seminuda* s.l. maxima observed at Hole 681B (Fig. 19), although there is no time frame known for the particular changes we observed.

At Hole 681B, the oxygen-minimum zone probably extended toward the shore several times, as indicated by the abundance pattern of *B. seminuda* s.l. (Fig. 19). Comparing selected faunal data from the three holes studied (Figs. 17 through 20) indicates that the oxygen-minimum zone may almost have reached Hole 679D (Fig. 20) during the last 730 k.y., when Groups E and F became more abundant and the *B. seminuda* s.l. maximum is documented. The subsequent increase of *Globobulimina* sp. (Fig. 20), following the *B. seminuda* s.l. maximum at Hole 679D, is explained by slightly improved bottom-water oxygenation because of a decrease in the surface-water productivity or a displacement of the high fertility zone due to a change in sea level.

Mapping changes in the abundance of *B. seminuda* s.l. at Hole 680B provided us with an excellent tool for tracing the geologic history of the oxygen-minimum zone. Changes in the distribution pattern of this key species suggest that the oxygen-minimum layer changed its position several times at this hole. The most frequently observed positions of the oxygen-minimum zone are shown in Figure 21A. This figure represents those time intervals when *B. seminuda* s.l. was abundant at Hole 680B. The increased abundance of this benthic species was probably favored by high surface-water fertility in combination with sluggish bottom-water circulation near Hole 680B. Figure 21B illustrates conditions when surface-water

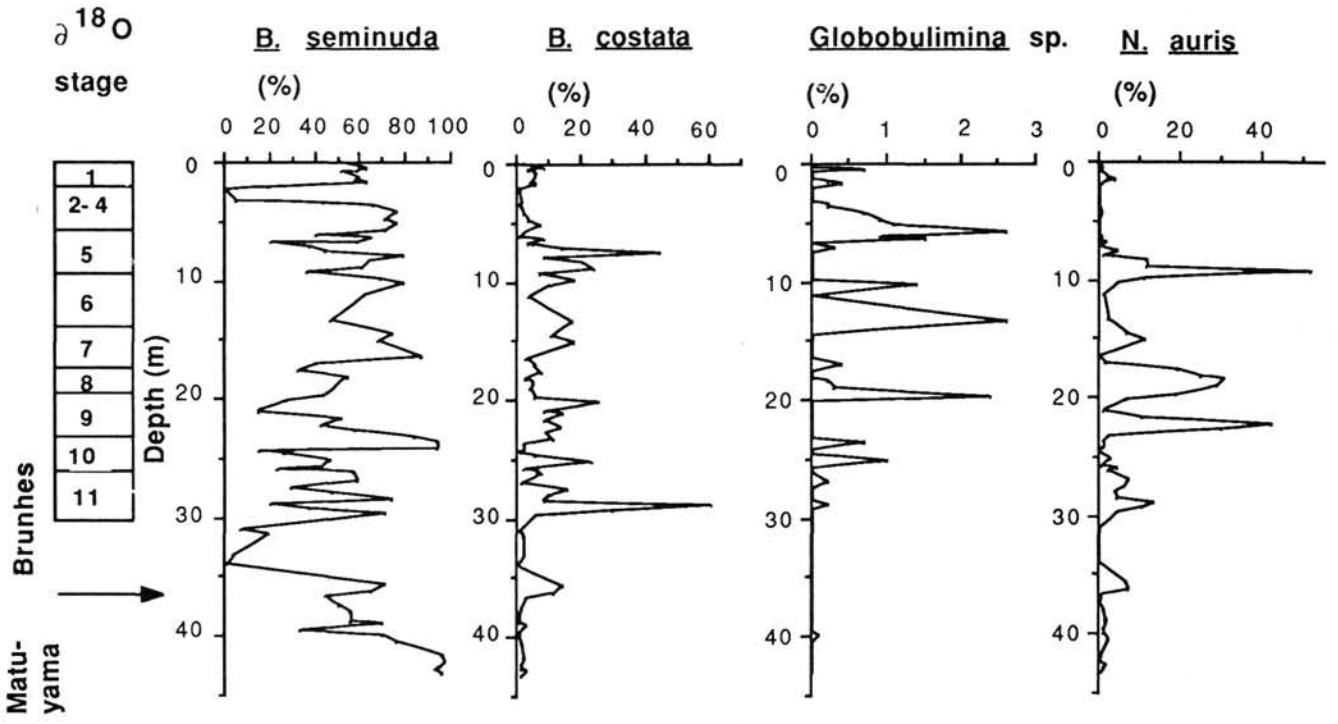

Figure 17. Distribution of selected benthic foraminifers tracing changes in the bottom-water oxygenation at Hole 680B during the last 423,000 yr.

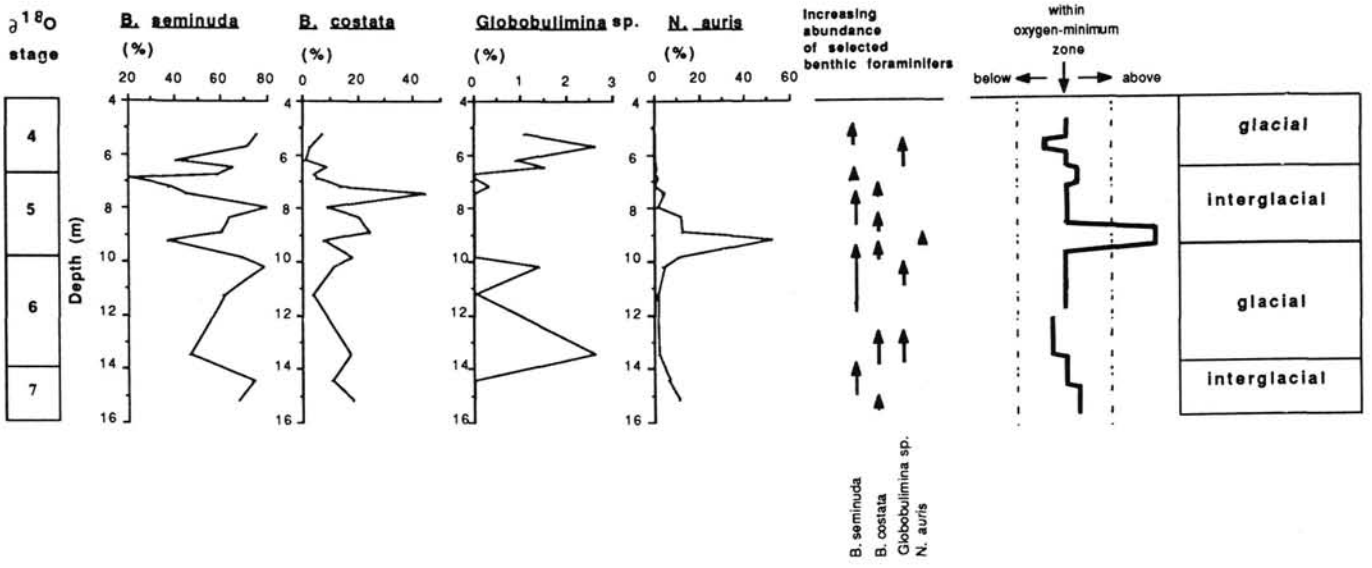

Figure 18. Distribution of selected benthic foraminifers, tracing bottom-water environmental changes at Hole 680B for the time interval, 60,000 to 200,000 yr.

fertility reached maximum values nearest the shore. These conditions probably represent times of extremely high fertility and high sea levels. As a consequence, the high fertility center moved in the direction of the coast. The oxygen-minimum layer intensified and may have shoaled and thus intersected the bottom nearer the shore in response to increased oxidation of organic matter derived from the photic zone (Fig. 21C).

A very different bottom-water environment is illustrated in Figures 21C and 21D, where oxygen depletion is less severe than in the cases discussed previously. The situation documented at Figure 21C may have occurred when sea level was lowered. As a consequence, both the high fertility zone and the oxygen-minimum zone were moved away from the former shoreline. The position of the holes drilled, however, does not yet allow for any conclusion upon strengthening of upwelling or shifting direction of the upwelling center during glacial/interglacial changes.

The situation documented in Figure 21D may have occurred when surface-water fertility decreased considerably and/or bottom currents supplied well-oxygenated water to the sedimentary environment on the shelf. The occurrence of abundant *N. auris*, e.g., during Stage 5, may record these conditions.

The increased abundance of *B. seminuda* s.l. at approximately 2.5 mbsf at Hole 679D indicates that the oxygen-minimum zone shifted vertically and/or thickened at least once to almost intersect the bottom topography at the upper-

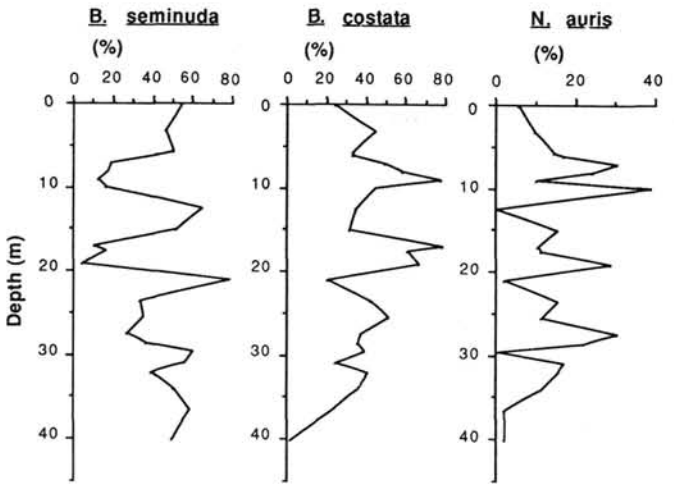

Figure 19. Distribution of selected benthic foraminifers, revealing changes in the bottom-water environment at Hole 681B.

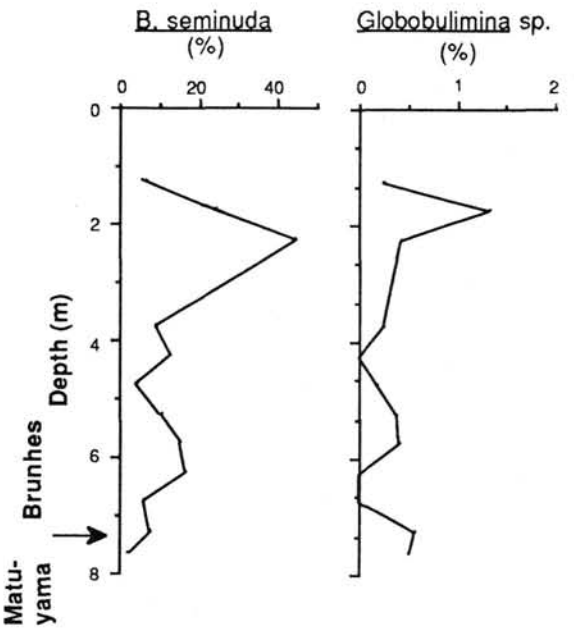

Figure 20. Distribution of selected benthic foraminiferal species, documenting changes in the bottom-water environment at Hole 679D.

slope location of Hole 679D. The oxygen-minimum zone may have been displaced by a lowering of the sea levels during a glacial interval (Fig. 21C). If our interpretation is valid, it would indicate that only one glacial interval is documented in the studied section of Hole 679D.

SUMMARY

At Hole 680B, upwelling intensity is interpreted to have been highest during the lower part of Stage 1, Stage 3, the upper part of Stage 5, and during the lower parts of Stages 6 and 7. Based on investigations of Holes 679D, 680B, and 681B, we conclude that the high-fertility center shifted offshore when maximum values for *B. seminuda* were observed at Hole 679D. This shift could have been due to a lowering of

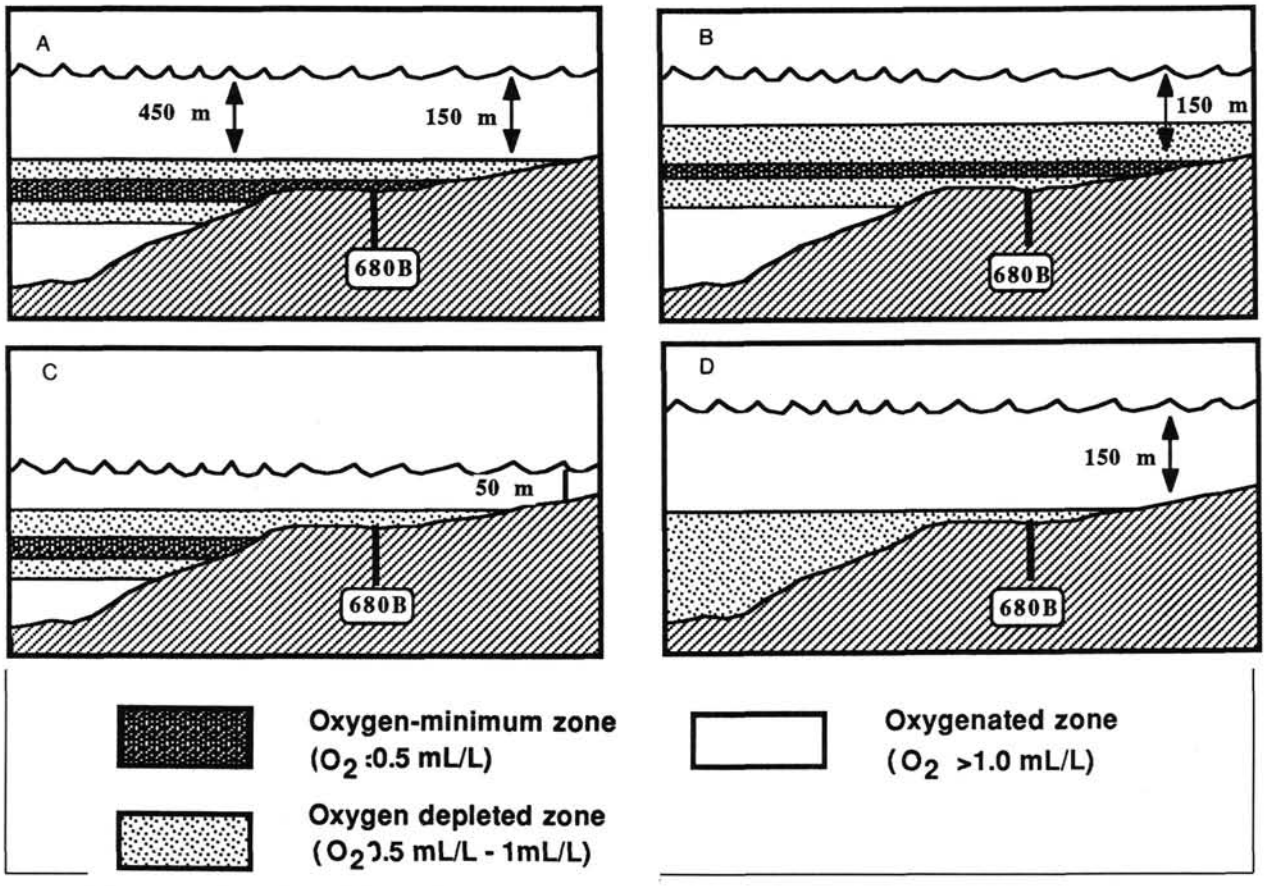

Figure 21. Schematic illustrations of the position of the oxygen-minimum layer at Hole 680B for different environmental settings (see text for further explanations).

sea level. With the limited stratigraphic information, however, we are not able to date this particular time slice properly.

Slowdowns of upwelling are documented within Stage 1, the upper part of Stages 2 through 4 and 7, the middle part of 6, and during Stage 9.

The levels of bottom-water oxygenation were lowest when *B. seminuda* showed maximum values. Oxygenation improved drastically when *N. auris* reached maximum values. This change most probably was caused by both mechanisms when (1) bottom-current activity increased and (2) surface-water productivity decreased (El-Niño-type events ?). After this event, high upwelling was again established, and *B. seminuda* reached maximum values (Figs. 17 through 19). Subsequently, when *B. costata* and *Globobulimina* sp. became more abundant, productivity in the surface water decreased again at the sites studied, although this decrease was less severe than during the presence of *N. auris*.

Displacement of the oxygen-minimum zone (as documented at Hole 680B) may relate to either a decrease in surface-water fertility, a glacio-eustatic change in sea level, and/or an increase in bottom-current activity. All processes can provide more oxygen to an earlier, poorly oxygenated, bottom-water layer. Off Peru, these mechanisms were probably effective, although for most time intervals no control exists for which of the process(es) were in action.

ACKNOWLEDGMENTS

We thank Edith Müller-Merz for inspiring comments on a first draft. Many thanks to Mona Botros and an anonymous reviewer, who made the manuscript readable and more understandable to English-speaking scientists. Suggestions and questions put forward by two anonymous reviewers improved discussion and made it more perspicuous.

REFERENCES

Bandy, O. L., and Rodolfo, K. S., 1964. Distribution of foraminifera and sediments, Peru-Chile trench area. *Deep-Sea Res.*, 11:817–837.

Bremner, J. M., 1983. Biogenic sediments on the Southwest African (Namibian) continental margin. *In* Thiede, J., and Suess, E. (Eds.), *Coastal Upwelling, Its Sedimentary Record. Part B: Sedimentary Records of Ancient Coastal Upwelling*. NATO Conf. Ser. IV, Mar. Sci., 10:73–103.

Brockmann, C., Fahrbach, E., Huyer, A., and Smith, R. L., 1980. The poleward undercurrent along the Peru coast: 5° to 15°S. *Deep-Sea Res.*, 27(A):847–856.

Calvert, S. E., 1966. Accumulation of diatomaceous silica in the sediments of the Gulf of California. *Bull. Geol. Soc. Am.*, 77:569–596.

Chappell, J., and Shackleton, N. J., 1986. Oxygen isotopes and sea level. *Nature*, 324:137–140.

DeVries, T. J., and Pearcy, W. G., 1982. Fish debris in sediments of the upwelling zone off central Peru. *Deep-Sea Res.*, 28(A):87–109.

Hart, T. J., and Currie, R. J., 1960. The Benguela Current. *Discovery Rept.*, 31:123–298.

Imbrie, J., Hays, J. D., Martinson, D. G., McIntyre, A., Mix, A. C., Morley, J. J., Pisias, N. G., Prell, W. L., and Shackleton, N. J., 1984. The orbital theory of Pleistocene climate: Support from a revised chronology of the $\delta^{18}O$ record. *In* Berger et al. (Eds.), *Milankovitch and Climate, Part 1:* New York (Riedel Publ.), 269–305.

Ingle, J. C., Jr., Keller, G., and Kolpack, R. L., 1980. Benthic foraminiferal biofacies, sediments and water masses of the southern Peru-Chile trench area, southeastern Pacific Ocean. *Micropaleontology*, 26(2):113–150.

Krissek, L. A., and Scheidegger, K. F., 1983. Environmental controls on sediment texture and composition in low oxygen zones off Peru and Oregon. *In* Thiede, J., and Suess, E. (Eds.), *Coastal Upwelling, Its Sedimentary Record. Part B: Sedimentary Records of Ancient Coastal Upwelling*. NATO Conf. Ser. IV, Mar. Sci., 10:163–180.

Kulm, L. D., Schrader, H., Resig, J. M., Thornburg, T. M., Masias, A., and Johnson, L., 1981. Late Cenozoic carbonates on the Peru continental margin: lithostratigraphy, biostratigraphy, and tectonic history. *In* Kulm, L. D., Dymond, J., Dasch, E. J., and Hussong, D. M. (Eds), *Nazca Plate: Crustal Formation and Andean Convergence*. Geol. Soc. Am. Mem., 154:469–508.

Lutze, G. F., 1962. Variationsstatistik und ökologie bei rezenten Foraminiferen. *Paleontol. Ztsch.*, 36:252–264.

_____, 1964. Statistical investigations on the variability of *Bolivina argentea*. *Cushman Contr. Cushman Found. Foram. Res. Contr.*, 15/3:105–116.

Molina-Cruz, A., 1977. The relation of the southern trade winds to upwelling processes during the last 75,000 years. *Quat. Res.*, 8:324–338.

_____, 1984. Radiolaria as indicators of upwelling processes: The peruvian connection. *Mar. Micropaleontol.*, 9:63–75.

Müller, P. J., and Suess, E., 1979. Productivity, sedimentation rate, and sedimentary organic matter in the oceans: I. Organic carbon preservation. *Deep-Sea Res.*, 26A:1347–1362.

Phleger, F. B., and Soutar, A., 1973. Production of benthic foraminifers in three east Pacific oxygen minima. *Micropaleontology*, 19/1:110–115.

Quinn, W. H., Zopf, D. O., Short, K. S., and Kuo Yang, R.T.W., 1978. Historical trends and statistics of the southern oscillation, El Niño, and Indonesian draughts. *Fishery Bull.*, 76/3:663–678.

Quintero, P. J., and Gardner, J. V., 1987. Benthic foraminifers on the continental shelf and upper slope, Russian River area, northern California. *J. Foramin. Res.*, 17/2:132–152.

Reid, J. L., 1959. Evidence of a South Equatorial Countercurrent in the Pacific Ocean. *Nature*, 184:209–210.

Reid, J. L., 1973. The shallow salinity-maximum of the Pacific Ocean. *Deep-Sea Res.*, 20:51–68.

Reimers, C. E., and Suess, E., 1983. Spatial and temporal patterns of organic matter accumulation on the Peru continental margin. *In* Suess, E., and Thiede, J. (Eds.), *Coastal Upwelling, Its Sediment Record: Part A: Responses of the Sedimentary Regime to Present Coastal Upwelling*. NATO Conf. Ser. IV, Mar. Sci., 10A:311–346.

Resig, J. M., 1976. Benthic foraminiferal stratigraphy, eastern margin, Nazca Plate. *In* ●●●●, et al., *Init. Repts. DSDP.*, 34: Washington (U.S. Govt. Printing Office), 743–760.

Romine, K., and Moore, T. C., Jr., 1981. Radiolarian distributions and paleoceanography of the eastern Equatorial Pacific Ocean during the last 127,000 years. *Palaeogeogr., Palaeoclimat., Palaeoecol.*, 35:281–314.

Sarnthein, M., 1971. *Oberflächensedimente im Persischen Holf und Golf von Oman II. Quantitative Komponentenanalyse der Grobfraktion. Deutsche Forschungsgemeinschft, "Meteor" Forschungsergebn., Reihe C/5:* Berlin (Gebrüder Bornträger), 1–113.

Sarnthein, M., Thiede, J., Pflaumann, U., Erlenkeuser, H., Fütterer, D., Koopmann, B., Lange, H., and Seibold, E., 1982. Atmospheric and oceanic circulation patterns off northwest Africa during the past 25 million years. *In* von Rad, U., Hinz, K., Sarnthein, M., and Seibold, E. (Eds.), *Geology of the Northwest African Continental Margin:* New York-Berlin-Heidelberg (Springer-Verlag), 545–604.

Shackleton, N. J., 1977. The oxygen isotope stratigraphic record of the Late Pleistocene. *Phil. Trans. R. Soc. London*, 280:169–182.

Smith, P. B., 1963. Quantitative and qualitative analysis of the family Bolivinidae: Recent foraminifera off Central America. *U.S. Geol. Surv. Prof. Pap.*, 429(A):A1–A35.

_____, 1964. Ecology of benthonic species: Recent foraminifera off Central America. *U.S. Geol. Surv. Prof. Pap.*, 429(B):B1–B51.

Smith, R. L., 1983. Circulation patterns in upwelling regimes. *In* Suess, E., and Thiede, J. (Eds.), *Coastal Upwelling, Its Sediment Record. Part A: Responses of the Sedimentary Regime to Present Coastal Upwelling*. NATO Conf. Ser. IV, Mar. Sci., 10A:13–36.

Suess, E., Kulm, L. D., and Killingly, J. S., 1986. Coastal upwelling and the history of organic-rich mudstone deposition off Peru. *In* Brooks, J., and Fleet, A. J., (Eds.), *Marine Petroleum Source Rocks*. Geol. Soc. Am., Spec. Publ., 24:181–197.

Suess, E., von Huene, R. et al., 1988. *Proc ODP, Init. Repts.*, 112: College Station, TX (Ocean Drilling Program).

Wyrtki, K., 1962. The oxygen minima in relation to ocean circulation. *Deep-Sea Res.*, 9:11–23.

_____, 1967. Circulation and water masses in the eastern Equatorial Pacific ocean. *Int. J. Oceanogr. Limnol.*, 1:117–147.

Date of initial receipt: 26 October 1988
Date of acceptance: 13 July 1989
Ms 112B-166

Appendix A. Abundances of components in the >63-μm size fraction at Hole 680B for the last 730,000 yr.

Site	Core/ sect.	Interval (cm)	Depth (m)	Plankt. f. (%)	Benth. f. (%)	Rads. (%)	Diat. (%)	Fish	Rem. (%)	Aggr. (%)	Phosph. (%)	Terr. (%)
680B	1H-1	4	0.03	0	23	8	0	25	33	0	10	
680B	1H-1	18–22	0.18	0	7	12	0	35	42	0	5	
680B	1H-1	23–27	0.23	0	0	10	0	54	29	0	8	
680B	1H-1	35–39	0.35	0	5	19	1	35	30	0	10	
680B	1H-1	40–41	0.40	0	5	14	1	50	16	0	14	
680B	1H-1	48–52	0.48	0	5	27	8	36	20	0	3	
680B	1H-1	52–53	0.52	0	16	11	4	35	29	0	5	
680B	1H-1	65–66	0.65	2	46	4	19	14	14	0	1	
680B	1H-1	73–77	0.73	1	28	8	4	42	10	0	7	
680B	1H-1	87–88	0.87	0	45	13	9	19	11	0	4	
680B	1H-1	112–113	1.12	0	10	9	1	46	29	0	5	
680B	1H-1	123–125	1.23	0	22	17	2	32	8	0	20	
680B	1H-1	131–132	1.31	3	41	9	2	26	7	0	12	
680B	1H-1	146–150	1.46	0	29	18	1	33	11	0	9	
680B	1H-2	3	1.54	0	4	5	0	27	55	0	10	
680B	1H-2	14–16	1.64	3	49	4	4	26	6	0	8	
680B	1H-2	23–27	1.73	1	12	14	0	25	40	0	8	
680B	1H-2	29–31	1.79	2	59	11	2	4	14	0	7	
680B	1H-2	41–43	1.91	0	30	17	1	19	21	0	12	
680B	1H-2	48–52	1.98	0	5	17	0	29	28	0	21	
680B	1H-2	54–56	2.04	0	14	14	0	36	13	0	23	
680B	1H-2	73–77	2.23	0	1	20	0	53	1	1	25	
680B	1H-2	79–81	2.29	0	0	10	0	49	15	1	25	
680B	1H-2	91–93	2.41	1	49	0	0	26	2	0	21	
680B	1H-2	98–102	2.49	0	0	13	0	32	32	0	23	
680B	1H-2	113–115	2.63	0	0	18	0	49	11	0	22	
680B	1H-2	123–127	2.73	0	0	13	0	61	1	0	25	
680B	1H-2	134–136	2.84	0	0	19	0	56	0	0	25	
680B	1H-3	23–27	3.23	15	36	1	0	12	11	0	24	
680B	1H-3	39–40	3.39	0	1	3	0	68	3	0	26	
680B	1H-3	48–52	3.48	14	34	0	0	20	8	0	23	
680B	1H-3	73–77	3.73	8	46	2	13	15	6	0	10	
680B	1H-3	83–84	3.83	1	27	1	4	49	6	0	12	
680B	1H-3	98–102	3.98	0	8	3	36	40	3	0	11	
680B	1H-3	109–110	4.09	0	3	17	5	38	20	0	16	
680B	1H-3	123–127	4.23	6	44	1	10	29	7	0	2	
680B	1H-3	146–150	4.46	1	16	1	26	36	17	0	2	
680B	1H-4	23–27	4.73	3	27	6	9	46	9	0	7	
680B	1H-4	43–44	4.93	0	51	4	26	12	1	0	6	
680B	1H-4	48–52	4.98	0	19	5	11	52	9	0	5	
680B	1H-4	73–77	5.23	0	38	3	31	18	8	0	2	
680B	2H-1	23–27	5.73	1	55	10	7	19	5	0	2	
680B	2H-1	40–41	5.90	0	52	4	3	23	14	0	5	
680B	2H-1	48–50	5.98	0	32	5	0	11	50	0	1	
680B	2H-1	73–77	6.23	0	76	5	30	11	3	0	1	
680B	2H-1	87–88	6.37	0	50	5	4	37	5	0	1	
680B	2H-1	98–102	6.48	1	85	5	0	4	3	0	2	
680B	2H-1	123–127	6.73	8	51	0	31	2	6	0	1	
680B	2H-1	138–139	6.88	0	35	2	1	16	45	0	1	
680B	2H-1	146–150	6.96	0	5	3	0	2	87	0	3	
680B	2H-2	23–27	7.23	0	46	4	1	17	28	0	4	
680B	2H-2	40–41	7.40	0	26	3	0	48	8	1	16	
680B	2H-2	48–52	7.48	0	42	2	21	10	22	0	3	
680B	2H-2	73–77	7.73	4	63	2	1	2	28	0	1	
680B	2H-2	88–89	7.88	19	70	3	0	3	5	0	1	
680B	2H-2	98–102	7.98	6	59	1	1	4	27	0	1	
680B	2H-2	123–127	8.23	38	2	0	41	0	19	0	0	
680B	2H-2	135–136	8.35	44	19	1	13	1	21	0	0	
680B	2H-2	146–150	8.46	32	15	1	29	0	23	0	0	
680B	2H-3	23–27	8.73	43	29	1	16	0	10	0	0	
680B	2H-3	40–41	8.90	44	30	1	7	0	17	0	0	
680B	2H-3	48–52	8.98	38	28	0	6	1	27	0	0	
680B	2H-3	73–77	9.23	43	28	0	16	0	13	0	0	
680B	2H-3	88–89	9.38	37	39	1	2	3	16	0	2	
680B	2H-3	98–102	9.48	31	49	0	0	3	15	0	1	
680B	2H-3	123–127	9.73	2	37	4	0	46	8	0	3	
680B	2H-3	135–136	9.85	8	50	1	1	15	22	0	3	
680B	2H-3	146–150	9.96	0	2	3	1	15	78	0	1	
680B	2H-4	23–27	10.23	1	35	4	8	40	8	0	5	
680B	2H-4	48–52	10.48	0	0	8	0	61	9	0	23	
680B	2H-4	73–77	10.73	0	0	5	0	70	0	1	25	
680B	2H-4	98–102	10.98	0	35	3	21	23	18	0	1	
680B	2H-4	123–127	11.23	0	81	0	18	0	0	0	0	
680B	2H-4	146–150	11.46	0	1	16	0	56	20	0	6	
680B	2H-5	23–27	11.73	0	0	21	9	63	5	0	3	
680B	2H-5	48–52	11.98	0	0	18	18	31	31	0	2	
680B	2H-5	73–77	12.23	0	0	18	12	28	36	0	5	

Appendix A (continued).

Site	Core/ sect.	Interval (cm)	Depth (m)	Plankt. f. (%)	Benth. f. (%)	Rads. (%)	Diat. (%)	Fish	Rem. (%)	Aggr. (%)	Phosph. (%)	Terr. (%)
680B	2H-5	98–102	12.48	0	0	20	1	56	14	0	9	
680B	2H-5	123–127	12.73	0	0	13	6	59	16	0	6	
680B	2H-5	146–150	12.96	0	0	30	10	43	7	0	10	
680B	2H-6	23–27	13.23	0	3	12	5	42	28	0	11	
680B	2H-6	48–52	13.48	2	38	9	31	10	10	0	1	
680B	2H-6	73–77	0	0	13	5	30	45	0	8		
680B	2H-6	123–127	14.23	0	20	1	48	28	0	0	2	
680B	2H-6	146–150	14.46	4	29	3	34	28	1	0	1	
680B	2H-7	23–27	14.73	0	6	0	37	19	1	19	17	
680B	2H-7	48–52	14.98	0	0	13	0	38	40	0	8	
680B	2H-7	66–70	15.16	6	80	1	0	5	5	0	2	
680B	3H-1	23–27	15.23	2	7	19	1	36	31	0	4	
680B	3H-1	48–52	15.48	0	0	2	6	14	74	0	5	
680B	3H-1	73–77	15.73	0	0	5	18	56	6	0	15	
680B	3H-1	98–102	15.98	0	0	1	1	66	3	0	29	
680B	3H-1	123–127	16.23	0	0	8	3	28	46	0	16	
680B	3H-1	146–150	16.46	0	4	3	2	22	67	0	3	
680B	3H-2	23–27	16.73	14	15	0	68	0	2	0	0	
680B	3H-2	48–52	16.98	3	58	0	0	3	33	0	3	
680B	3H-2	73–77	17.23	0	0	8	0	14	63	0	16	
680B	3H-2	98–102	17.48	0	0	4	3	25	67	0	1	
680B	3H-2	123–127	17.73	8	32	5	0	8	20	1	28	
680B	3H-2	146–150	17.96	3	25	1	0	25	23	0	24	
680B	3H-3	23–27	18.23	7	74	1	1	5	7	0	3	
680B	3H-3	48–52	18.48	4	56	0	17	2	20	0	1	
680B	3H-3	73–77	18.73	0	31	1	0	17	23	0	27	
680B	3H-3	98–102	18.98	0	67	6	0	12	13	0	1	
680B	3H-3	110–114	19.10	0	82	1	4	1	9	0	1	
680B	3H-4	23–27	18.73	1	72	7	0	8	13	0	0	
680B	3H-4	48–52	19.98	0	4	0	0	0	95	0	2	
680B	3H-4	73–77	20.23	0	36	6	0	31	21	0	5	
680B	3H-4	98–102	20.48	0	37	7	0	3	50	0	3	
680B	3H-4	123–127	20.73	0	15	3	0	14	51	0	17	
680B	3H-4	146–150	20.96	2	32	0	0	33	0	0	33	
680B	3H-5	23–27	21.23	3	56	1	0	8	9	0	22	
680B	3H-5	48–52	21.48	0	0	2	0	0	96	0	1	
680B	3H-5	73–77	21.73	1	82	5	0	2	9	0	1	
680B	3H-5	98–102	21.98	27	29	3	3	3	37	0	0	
680B	3H-5	123–127	22.23	43	27	2	2	2	23	0	1	
680B	3H-5	146–150	22.46	21	33	1	1	1	44	0	0	
680B	3H-6	23–27	22.73	38	38	2	7	1	10	0	3	
680B	3H-6	48–52	22.98	0	1	46	0	5	38	0	12	
680B	3H-6	73–77	23.23	0	20	2	0	8	66	0	5	
680B	3H-6	98–102	23.48	0	0	4	0	37	59	0	0	
680B	3H-6	123–127	23.73	8	55	0	19	10	8	0	0	
680B	3H-6	146–150	23.96	0	0	8	9	63	20	0	1	
680B	3H-7	23–27	24.23	0	9	3	0	63	5	0	21	
680B	3H-7	48–52	24.48	5	70	0	0	0	2	0	23	
680B	3H-7	62–66	24.62	13	64	0	0	0	0	0	24	
680B	4H-1	23–27	24.73	3	59	0	0	1	14	0	24	
680B	4H-1	48–52	24.98	1	56	0	0	1	19	0	23	
680B	4H-1	73–77	25.23	2	76	2	0	0	14	0	5	
680B	4H-1	98–102	25.48	4	67	0	0	2	4	0	23	
680B	4H-1	123–127	25.73	1	70	0	0	1	5	0	23	
680B	4H-1	146–150	25.96	5	26	1	0	30	17	0	20	
680B	4H-2	23–27	26.23	0	70	3	0	14	12	0	1	
680B	4H-2	48–52	26.48	0	32	2	0	0	66	0	0	
680B	4H-2	73–77	26.73	5	85	2	1	4	2	0	0	
680B	4H-2	98–102	26.98	0	81	0	15	1	3	0	0	
680B	4H-2	123–127	27.23	2	85	0	0	5	4	0	4	
680B	4H-2	146–150	27.46	43	28	0	0	0	15	0	15	
680B	4H-3	23–27	27.73	13	64	1	0	9	1	0	12	
680B	4H-3	48–52	27.98	11	32	1	0	32	2	0	21	
680B	4H-3	73–77	28.23	3	83	1	0	1	1	0	11	
680B	4H-3	98–102	28.48	3	78	0	0	0	18	0	1	
680B	4H-3	123–127	28.73	2	70	3	0	4	20	0	1	
680B	4H-3	146–150	28.96	1	32	0	2	5	42	0	18	
680B	4H-4	23–27	29.23	2	77	1	0	4	16	0	1	
680B	4H-4	48–52	29.48	0	1	0	0	25	74	0	0	
680B	4H-4	73–77	29.73	3	65	2	0	0	29	0	1	
680B	4H-4	98–102	29.98	2	4	2	0	3	90	0	0	
680B	4H-4	123–127	30.23	0	2	4	0	63	7	0	25	
680B	4H-4	146–150	30.46	0	0	0	0	0	100	0	0	
680B	4H-5	23–27	30.73	0	0	9	0	39	34	0	10	
680B	4H-5	48–52	30.98	4	43	0	0	2	28	1	22	
680B	4H-5	73–77	31.23	20	57	0	0	0	1	0	22	
680B	4H-5	98–102	31.48	8	75	0	0	0	0	0	18	

Appendix A (continued).

Site	Core/ sect.	Interval (cm)	Depth (m)	Plankt. f. (%)	Benth. f. (%)	Rads. (%)	Diat. (%)	Fish	Rem. (%)	Aggr. (%)	Phosph. (%)	Terr. (%)
680B	4H-5	123–127	31.73	0	2	4	0	21	49	0	23	
680B	4H-5	146–150	31.96	0	0	0	0	2	93	0	5	
680B	4H-6	23–27	32.23	0	0	8	0	7	56	0	28	
680B	4H-6	48–52	32.48	3	0	5	0	1	47	0	45	
680B	4H-6	73–77	32.73	0	0	0	0	0	67	0	33	
680B	4H-6	98–102	32.98	0	0	0	0	0	95	0	5	
680B	4H-6	123–127	33.23	18	56	0	0	0	7	0	18	
680B	4H-6	146–150	33.46	0	0	0	0	45	31	0	24	
680B	4H-7	23–27	33.73	22	55	0	0	0	5	0	18	
680B	4H-7	48–52	33.98	23	51	0	0	0	10	0	17	
680B	5H-1	23–27	34.23	0	0	6	13	43	29	0	9	
680B	5H-1	48–50	34.48	0	0	3	4	35	50	0	9	
680B	5H-1	73–77	34.73	0	0	0	0	50	0	1	49	
680B	5H-1	98–102	34.98	0	0	0	1	25	71	0	2	
680B	5H-1	123–127	35.23	0	0	4	0	45	37	0	14	
680B	5H-1	146–150	36.46	0	0	0	0	53	10	11	26	
680B	5H-2	23–27	35.73	1	39	2	0	40	14	0	3	
680B	5H-2	48–52	35.98	0	3	0	0	3	92	0	2	
680B	5H-2	73–77	36.23	0	33	3	0	58	4	0	4	
680B	5H-2	123–127	36.73	1	17	1	0	43	10	4	25	
680B	5H-2	146–150	36.96	0	0	0	57	36	5	0	1	
680B	5H-3	23–27	37.23	0	0	10	18	58	13	0	3	
680B	5H-3	48–52	37.48	0	62	1	22	14	1	0	0	
680B	5H-3	73–77	37.73	0	0	1	36	42	23	0	0	
680B	5H-3	98–102	37.98	0	63	2	8	15	12	0	1	
680B	5H-3	123–127	38.23	0	0	9	3	38	45	0	5	
680B	5H-4	23–27	38.73	0	65	3	3	18	10	0	3	
680B	5H-4	48–52	38.98	0	70	3	8	8	11	0	1	
680B	5H-4	73–77	39.23	0	5	6	4	74	10	0	1	
680B	5H-4	98–102	39.48	0	20	3	19	48	11	0	0	
680B	5H-4	123–127	39.73	0	5	10	18	55	10	0	3	
680B	5H-4	146–150	39.96	0	71	2	1	13	13	0	1	
680B	5H-5	23–27	40.23	0	25	0	0	50	1	1	23	
680B	5H-5	48–52	40.48	0	38	1	0	12	19	3	26	
680B	5H-5	73–77	40.73	0	12	4	0	61	0	1	22	
680B	5H-5	98–102	40.98	0	0	4	3	61	5	4	24	
680B	5H-5	123–127	41.23	0	2	1	23	50	1	2	22	
680B	5H-5	146–150	41.46	0	4	3	4	59	1	6	24	
680B	5H-6	23–27	41.73	0	10	1	9	57	0	2	22	
680B	5H-6	48–52	41.98	0	21	0	0	51	3	3	23	
680B	5H-6	73–77	42.23	0	20	1	3	50	0	4	23	
680B	5H-6	123–127	42.73	0	15	1	1	55	0	4	24	
680B	5H-6	146–150	42.96	0	13	0	3	58	0	5	23	
680B	5H-7	23–27	43.23	0	9	1	0	54	0	13	24	

Appendix B. Abundances of components in the >40-μm size fraction of Core 112-680B-2H, representing the time interval 60,000 to 200,000 yr.

Site	Core/section	Interval (cm)	Depth (m)	Total counts	Diatoms	Radialarians	Benthic foram.	Plankt. foram.	Plank. fragm.	Fish remains	Phosph.	Quartz	Relict bio.	Pteropods	Gastropods
680B	2H-1	20–22	5.70	3139	320	110	1794	27	6	186	45	330	258	0	0
680B	2H-1	33–34	5.83	3076	391	278	1223	20	52	355	61	459	115	0	0
680B	2H-1	57–59	6.07	2782	533	486	829	4	37	383	45	323	103	0	0
680B	2H-1	82–83	6.32	2150	103	158	1505	14	35	235	84	460	328	0	0
680B	2H-1	115–117	6.65	3222	278	73	1566	95	35	247	121	521	257	0	0
680B	2H-2	20–22	7.20	2817	660	183	842	22	9	146	184	513	223	0	0
680B	2H-2	33–34	7.33	2365	24	277	214	6	0	486	224	850	21	0	0
680B	2H-2	57–59	7.57	2630	1357	42	313	5	3	56	44	706	13	0	0
680B	2H-2	82–83	7.82	3239	247	202	1700	54	22	420	27	205	394	0	0
680B	2H-2	115–117	8.15	3007	1861	63	404	280	31	34	13	78	68	202	0
680B	2H-3	20–22	8.70	2887	1316	110	410	418	80	77	14	163	105	147	4
680B	2H-3	33–34	8.83	2961	1006	147	499	388	53	163	40	289	112	187	11
680B	2H-3	57–59	9.07	3555	485	100	820	756	146	129	69	431	131	370	13
680B	2H-3	82–83	9.32	3181	1500	71	555	551	90	60	3	175	37	61	5
680B	2H-3	115–117	9.65	3317	92	130	1717	87	113	453	39	226	418	9	0
680B	2H-4	20–22	10.20	2898	799	137	884	23	19	577	37	245	137	0	0
680B	2H-4	33–34	10.33	2166	515	428	31	1	1	64	83	898	8	0	0
680B	2H-4	57–59	10.57	2610	752	294	10	1	0	325	36	979	9	0	0
680B	2H-4	82–83	10.82	3544	34	52	0	0	0	1498	89	1431	2	0	0
680B	2H-4	115–117	11.15	2810	177	98	1674	18	4	142	5	172	471	0	0
680B	2H-5	20–22	11.70	2715	1250	286	667	11	8	242	12	106	16	0	0
680B	2H-5	33–34	11.83	2495	1283	585	2	1	0	46	27	458	6	0	0
680B	2H-5	57–59	12.07	2548	1262	174	1	0	0	214	66	707	6	0	0
680B	2H-5	82–83	12.32	2531	1087	500	0	0	0	0	42	760	9	0	0
680B	2H-5	115–117	12.65	2470	1896	313	0	1	1	42	12	164	2	0	0
680B	2H-6	15–17	13.15	2389	961	263	0	1	0	318	61	627	5	0	0
680B	2H-6	33–34	13.33	2419	1025	253	24	0	0	559	69	397	11	0	0
680B	2H-6	57–59	13.57	2566	1411	128	378	1	1	263	33	177	135	0	0
680B	2H-6	82–83	13.82	2619	1762	40	388	97	13	19	36	140	88	0	0
680B	2H-6	115–117	14.15	2908	999	75	513	12	2	474	80	469	107	0	0
680B	2H-7	5	14.55	2631	1830	15	46	0	0	26	50	356	11	0	0
680B	2H-7	33–34	14.83	2508	2037	178	0	0	0	36	43	166	1	0	0
680B	2H-7	57–59	15.07	2792	323	187	1521	30	41	138	29	258	198	0	0

Appendix C. Analyses of the benthic foraminifer assemblage at Hole 679D.

Site	Core/ section	Interval (cm)	Depth (m)	Total benth. f.	*B. costata*	*B. minuta*	*B. interj.*	*B. plicata*	*B. seminuda* s.l.	*B. sinuata*	*B. spissa*	*B. curta*	*B. elegant.*	*C. auricula*	*B. subfusi.*	*C. cushmani*	*C. subglobatus*	*C. limbata*
679D	1H-1	124–127	1.24	411	2	72	12	0	28	0	11	8	0	2	0	0	19	0
679D	1H-2	23–27	1.73	896	9	29	10	0	212	2	3	0	1	10	40	2	3	0
679D	1H-2	73–77	2.23	460	7	5	14	16	204	0	0	7	2	8	0	0	1	2
679D	1H-3	73–77	3.73	1251	6	52	4	77	110	0	0	10	0	9	0	0	0	6
679D	1H-3	123–127	4.23	453	5	87	24	2	58	0	1	1	0	1	1	3	0	57
679D	1H-4	23–27	4.73	529	3	203	32	6	22	0	8	3	1	0	0	0	7	60
679D	1H-4	73–77	5.23	517	17	78	15	3	51	2	18	8	3	9	0	6	23	61
679D	1H-4	123–127	5.73	486	3	26	13	0	74	3	9	4	3	5	0	74	15	56
679D	1H-5	23–27	6.23	664	2	64	6	0	111	35	3	20	11	13	0	160	33	6
679D	1H-5	73–77	6.73	594	46	74	7	0	35	8	7	0	18	61	14	181	20	8
679D	1H-5	123–127	7.23	528	11	12	90	0	40	0	11	4	0	4	0	4	0	51

Site	Core/ section	Interval (cm)	Depth (m)	*E. bradyana*	*E. obesa*	*E. pacifica*	*Globobul.* spp.	*G. altiformis*	*G. rothwelli*	*Gyroidina* sp.	*S. eckisi*	*T. carinata*	*T. angulata*	*U. peregr.*	*V. inflata*	pl. forams	rads
679D	1H-1	124–127	1.24	0	26	50	1	0	2	0	0	11	0	46	7	17	22
679D	1H-2	23–27	1.73	144	108	0	12	1	70	0	0	19	3	57	2	69	13
679D	1H-2	73–77	2.23	70	47	2	2	3	0	0	0	5	4	21		61	29
679D	1H-3	73–77	3.73	750	107	60	3	0	31	0	0	4	1	3	6	10	0
679D	1H-3	123–127	4.23	72	3	32	0	0	45	0	2	19	3	0	10	237	1
679D	1H-4	23–27	4.73	51	4	4	1	0	89	10	0	7	1	0	4	232	0
679D	1H-4	73–77	5.23	59	49	0	2	0	38	35	5	16	13	0	6	204	0
679D	1H-4	123–127	5.73	0	0	43	2	4	66	14	8	14	5	0	5	115	4
679D	1H-5	23–27	6.23	0	12	0	0	8	48	53	0	16	0	48	4	14	0
679D	1H-5	73–77	6.73	0	0	0	0	7	34	14	10	0	0	31	2	33	1
679D	1H-5	123–127	7.23	0	0	0	3	0	55	17	62	18	0	12	64	62	3
679D	1H-6	13–17	7.63	11	4	4	2	0	73	12	1	28	0	17	31	643	0

Appendix D. Analyses of the benthic foraminifer assemblage at Hole 680B.

Site	Core/ section	Interval (cm)	Depth (m)	Plankt. f.	Pterop.	Total benth. f.	*B. alata*	*B. costata*	*B. interj.*	*B. plicata*	*B. salvad.*	*B. semin. h.*	*B. semin. s.*	*B. spissa*	*B.* sp.	*B. denudata*	*B. marginata*	*B. curta*	*C. auricula*	*C.* sp.	*C. cushmani*
680B	1H-01	3	0.03	0	0	69	0	1	0	17	0	35	0	0	0	0	0	1	1	1	0
680B	1H-01	35–39	0.35	0	0	141	4	12	0	10	0	84	0	0	0	0	0	2	8	0	0
680B	1H-01	52–53	0.52	3	0	296	4	11	0	17	0	186	0	0	0	0	0	10	6	0	0
680B	1H-01	73–77	0.73	1	0	434	0	26	0	40	0	254	0	0	0	0	0	4	21	0	0
680B	1H-01	87–88	0.87	6	0	402	2	22	0	62	0	209	0	0	0	0	0	10	15	0	0
680B	1H-01	131–132	1.31	7	0	361	6	19	0	14	0	219	0	0	0	0	0	4	2	0	0
680B	1H-02	14–16	1.64	26	3	459	2	20	0	3	0	266	0	0	0	0	0	2	1	0	0
680B	1H-02	29–31	1.79	5	0	240	2	13	0	31	0	151	0	0	0	0	0	2	12	0	0
680B	1H-02	54–56	2.04	0	0	482	0	2	0	256	0	93	0	0	0	0	0	14	37	0	0
680B	1H-02	91–93	2.41	0	0	270	0	2	0	66	0	1	0	0	0	0	0	1	0	0	0
680B	1H-03	23–27	3.23	11	0	337	0	5	1	25	0	17	0	0	0	0	0	0	2	0	0
680B	1H-03	48–52	3.48	34	0	458	0	2	0	14	0	201	0	0	0	0	0	2	0	0	0
680B	1H-03	73–77	3.73	12	0	423	0	5	0	9	0	278	0	0	0	0	0	10	0	0	0
680B	1H-03	123–127	4.23	8	0	273	0	6	0	0	0	207	0	0	0	0	0	0	0	0	0
680B	1H-04	43–44	4.93	8	0	432	0	14	1	24	0	307	0	0	0	0	0	14	1	0	0
680B	1H-04	73–77	5.23	3	0	358	0	25	0	9	0	270	0	0	0	1	0	9	0	0	0
680B	2H-01	23–27	5.73	1	0	392	1	9	0	30	0	278	0	0	0	0	0	30	1	0	0
680B	2H-01	73–77	6.23	2	0	327	3	3	0	83	0	133	0	0	0	0	0	13	3	0	0
680B	2H-01	98–102	6.48	2	0	403	0	34	0	10	0	262	0	0	0	0	0	13	1	0	0
680B	2H-01	123–127	6.73	0	0	132	0	5	1	13	0	77	0	0	0	0	0	1	0	0	0
680B	2H-01	138–139	6.88	3	0	355	11	17	0	65	0	72	0	0	0	0	0	16	5	0	0
680B	2H-02	23–27	7.23	0	0	673	0	93	0	202	0	253	0	0	0	0	0	7	7	0	0
680B	2H-02	48–52	7.48	0	0	400	0	177	0	3	0	176	0	0	0	0	0	0	2	0	0
680B	2H-02	98–102	7.98	4	0	502	0	42	0	5	0	397	0	0	0	0	0	0	4	0	0
680B	2H-02	135–136	8.35	91	41	340	0	69	0	0	0	217	0	0	0	0	0	0	0	1	0
680B	2H-03	40–41	8.9	252	88	572	0	138	0	0	0	345	0	0	0	0	0	0	0	0	1
680B	2H-03	73–77	9.23	39	11	283	0	21	0	0	0	103	0	0	0	0	0	0	0	0	0
680B	2H-03	135–136	9.85	18	0	217	0	38	0	0	0	148	0	0	0	0	0	0	0	0	0
680B	2H-04	23–27	10.23	9	0	221	0	24	0	0	0	173	0	0	0	0	0	0	0	0	0
680B	2H-04	123–127	11.23	10	0	244	0	9	0	10	0	149	0	0	0	0	0	0	3	0	0
680B	2H-06	48–52	13.48	34	0	191	0	33	1	0	0	88	0	0	0	0	0	2	1	0	0
680B	2H-06	146–150	14.46	24	0	274	0	29	0	0	0	202	0	0	0	0	0	0	0	0	0
680B	2H-07	66–70	15.16	14	0	355	0	64	0	0	0	240	0	0	0	0	0	0	2	0	0
680B	3H-01	146–150	16.46	0	0	312	0	9	0	7	0	279	0	0	0	0	0	2	11	0	0
680B	3H-02	48–52	16.98	3	0	278	1	15	0	0	0	112	0	0	0	0	0	0	34	0	3
680B	3H-02	123–127	17.73	17	0	219	0	17	0	0	0	70	0	0	0	0	0	0	0	0	0
680B	3H-03	23–27	18.23	33	0	447	0	13	0	0	0	243	0	0	0	0	0	3	0	0	3
680B	3H-03	48–52	18.48	28	0	569	0	27	0	0	0	295	0	0	0	0	0	0	3	0	0
680B	3H-03	98–102	18.98	6	0	310	0	14	0	1	0	151	0	0	0	0	0	5	3	0	0
680B	3H-04	23–27	19.73	0	0	336	0	18	0	0	0	147	0	0	0	0	0	13	6	0	2
680B	3H-04	73–77	20.23	7	0	323	0	82	0	4	0	89	0	0	0	0	0	22	13	2	0
680B	3H-04	146–150	20.96	2	0	359	0	30	0	0	0	54	0	0	0	0	0	3	3	1	6
680B	3H-05	23–27	21.23	9	0	578	0	82	1	4	1	89	0	13	0	0	0	1	0	0	1
680B	3H-05	73–77	21.73	2	0	462	0	39	0	0	0	239	0	0	0	0	0	2	10	0	4
680B	3H-05	123–127	22.23	89	26	448	0	60	0	0	0	192	0	0	0	0	0	1	0	0	2
680B	3H-06	23–27	22.73	33	12	324	0	30	0	0	0	188	0	0	0	0	0	0	0	0	0
680B	3H-06	73–77	23.23	1	0	194	0	22	1	0	0	162	0	0	0	0	0	0	1	0	0
680B	3H-06	123–127	23.73	2	0	268	0	5	0	0	0	252	0	0	0	0	0	0	0	0	0
680B	3H-07	23–27	24.23	3	0	173	0	4	0	0	0	162	0	0	0	0	0	0	0	0	0
680B	3H-07	48–52	24.48	50	0	382	0	0	3	0	0	3	54	0	0	0	0	0	0	0	0
680B	4H-01	23–7	24.73	9	0	477	0	28	9	68	0	70	56	0	0	0	0	0	0	1	0
680B	4H-01	73–77	25.23	8	0	291	0	68	1	5	0	136	0	0	0	0	0	0	18	0	10
680B	4H-01	123–127	25.73	3	0	494	0	11	2	88	0	60	147	0	0	0	0	1	0	0	119
680B	4H-01	146–150	25.96	30	0	300	0	19	3	11	0	59	10	0	0	0	0	7	2	0	80
680B	4H-02	23–27	26.23	1	0	320	0	25	1	15	0	181	0	0	0	0	0	5	4	0	42
680B	4H-02	98–102	26.98	2	0	501	0	7	0	6	0	290	0	0	0	0	0	5	10	0	7
680B	4H-02	146–150	27.46	386	0	163	0	25	0	2	0	47	0	0	0	0	0	0	0	0	3
680B	4H-03	48–52	27.98	111	0	353	0	38	2	18	0	158	8	0	0	0	0	2	2	0	11
680B	4H-03	98–102	24.48	12	0	279	0	23	0	0	0	207	0	0	0	0	0	0	0	9	6
680B	4H-03	146–150	28.96	9	0	402	0	245	1	0	1	79	0	0	0	0	0	0	4	0	1
680B	4H-04	23–27	29.23	10	0	401	0	120	0	2	0	149	0	0	0	0	0	8	37	0	7
680B	4H-04	73–77	29.73	21	0	430	0	24	0	4	0	306	0	0	0	0	0	3	20	0	22
680B	4H-05	48–52	30.98	223	0	483	0	2	22	1	2	0	33	6	0	0	0	0	0	0	0
680B	4H-05	98–102	31.48	46	0	414	0	8	4	101	0	0	79	0	0	1	2	0	4	0	0
680B	4H-06	123–127	33.23	194	0	424	0	9	0	37	4	2	15	8	0	0	0	0	0	0	0
680B	4H-07	48–52	33.98	445	0	325	0	0	1	15	1	0	3	40	0	0	0	0	3	0	0
680B	5H-02	23–27	35.73	29	0	540	0	76	0	1	0	376	0	0	0	0	1	7	0	0	0
680B	5H-02	73–77	36.23	8	0	564	0	64	0	0	0	362	0	0	0	0	0	1	3	0	0
680B	5H-02	123–127	36.73	16	0	322	0	10	0	0	0	18	126	0	0	0	0	1	0	0	0
680B	5H-03	48–52	37.48	1	0	480	0	8	0	0	0	241	3	0	0	0	0	194	0	0	0
680B	5H-03	98–102	37.98	1	0	616	0	6	0	0	0	342	0	0	0	0	0	127	0	0	0
680B	5H-04	23–27	38.73	6	0	625	0	4	0	0	0	350	0	0	0	0	0	122	0	0	0
680B	5H-04	48–52	38.98	3	0	559	0	14	0	0	0	389	0	0	0	2	0	82	0	0	0
680B	5H-04	98–102	39.48	1	0	448	0	3	0	0	0	139	10	0	0	11	0	239	0	0	0
680B	5H-04	146–150	39.96	1	0	686	0	5	0	0	0	479	0	0	0	5	0	163	0	0	0
680B	5H-05	48–52	40.48	1	0	358	0	4	0	0	0	269	0	0	0	0	0	0	0	0	1
680B	5H-06	23–27	41.73	0	0	329	0	8	0	0	0	317	0	0	0	0	0	1	0	0	0
680B	5H-06	73–77	42.23	1	0	303	0	4	0	0	0	295	0	0	0	0	0	0	0	0	0
680B	5H-06	123–127	42.73	0	0	190	0	3	0	0	0	181	0	0	0	0	0	0	0	0	0
680B	5H-06	146–150	42.96	0	0	302	0	9	0	0	0	280	0	0	0	0	0	0	0	0	0
680B	5H-07	23–27	43.23	0	0	374	0	5	0	0	0	357	0	0	0	0	0	0	0	0	0

Appendix D (continued).

C. subglob.	*C.* cf. *auka*	*C. tumida*	*E. bradyana*	*E. obesa*	*E.* cf. pacifica	*Globobul.* sp.	*Gyroi.* sp.	*N.* sp.	*N. stella*	*N. auris*	*S. eckisi*	*T. angulosa*	*T. carinata*	*U. peregrina*	*V. inflata*	*Virgul.* spp.	*Virguli-nella* spp.	*Stain-forthia* sp.
0	0	0	11	0	0	0	0	0	0	0	0	0	0	0	2	0	0	0
0	0	0	10	8	1	0	0	0	0	1	0	0	0	0	1	0	0	0
0	0	0	0	50	0	2	0	0	0	1	4	0	0	0	2	0	0	3
1	0	5	21	23	1	0	1	1	7	3	21	0	0	0	1	0	0	4
0	0	5	10	41	4	0	0	0	5	1	7	0	0	0	0	0	0	7
0	0	8	0	45	0	0	0	0	11	8	4	0	0	0	0	0	0	20
0	0	20	0	89	0	1	0	0	24	19	9	0	0	0	0	0	0	3
0	0	0	4	11	0	1	0	0	0	3	2	0	0	0	0	0	0	8
2	0	0	72	5	0	0	0	0	0	0	0	0	0	0	1	0	0	0
0	110	6	52	0	2	0	0	0	0	0	0	26	0	0	4	0	0	0
0	20	12	236	0	0	0	0	0	1	0	6	5	0	0	0	0	0	7
0	4	63	83	0	25	1	1	3	44	0	0	0	0	0	2	0	0	13
0	0	9	82	0	2	1	0	0	18	0	0	0	0	0	3	0	0	5
0	0	11	21	0	0	2	0	0	11	2	0	0	0	0	2	0	0	9
0	0	12	26	0	1	4	0	0	21	1	1	0	0	0	3	0	0	2
0	0	2	21	0	0	4	0	0	8	0	7	0	0	0	0	1	0	0
0	0	3	20	0	0	10	1	0	7	0	2	0	0	0	0	0	0	0
0	0	1	77	0	0	3	1	0	6	0	1	0	0	0	0	0	0	0
0	0	15	32	0	0	6	0	6	3	2	1	0	0	0	18	0	0	0
0	0	4	8	0	0	0	1	1	20	0	0	0	0	0	1	0	0	0
0	0	27	93	0	0	0	7	1	29	5	3	0	0	0	3	1	0	0
0	0	3	92	0	0	2	7	0	0	0	0	3	0	0	4	0	0	0
0	0	5	10	0	0	0	0	0	4	18	0	0	0	0	5	0	0	0
0	0	14	4	0	0	0	0	2	12	5	0	1	0	0	16	0	0	0
0	0	10	2	0	0	0	0	0	2	39	0	0	0	0	0	0	0	0
0	0	11	1	0	0	0	0	0	4	68	0	0	0	0	0	0	4	0
0	0	0	0	0	0	0	0	1	5	151	0	0	0	0	1	0	1	0
0	0	6	0	0	0	0	0	0	0	24	0	0	0	0	1	0	0	0
0	0	4	0	0	0	3	0	0	0	10	0	0	0	0	7	0	0	0
0	0	15	6	0	0	0	11	0	2	3	0	0	0	0	35	0	0	0
0	0	28	9	0	0	5	3	0	4	4	9	0	0	0	1	0	1	0
0	0	9	5	0	0	0	0	0	7	18	0	0	0	0	0	0	0	4
0	0	2	3	0	0	0	1	0	0	40	1	0	0	0	2	0	0	0
1	0	0	0	0	0	0	9	0	0	0	0	2	0	0	1	0	0	0
1	0	14	0	0	0	1	17	0	1	5	1	0	0	0	69	0	0	0
0	0	79	0	0	0	0	2	0	0	43	3	0	0	0	3	0	0	2
0	0	64	3	0	0	0	1	0	0	111	4	0	0	0	1	0	0	1
0	0	44	0	0	0	1	0	4	0	174	6	0	0	0	1	1	1	12
0	0	16	4	0	2	1	8	0	0	90	3	0	0	0	12	0	0	0
0	0	1	14	0	1	8	48	0	0	63	3	0	0	0	9	0	3	0
0	0	23	29	0	0	0	37	0	0	21	0	0	0	0	1	0	0	0
0	0	92	75	0	0	0	82	0	0	6	3	1	1	0	2	0	0	0
0	5	157	17	0	24	0	128	1	0	8	4	3	7	0	25	0	0	0
0	0	86	0	0	0	0	6	0	2	50	0	0	0	0	24	0	0	0
0	0	2	0	0	0	0	0	0	0	189	1	0	0	0	1	0	0	0
0	0	1	0	0	0	0	0	0	4	97	0	0	0	0	0	0	4	0
0	0	4	0	0	0	0	0	0	0	4	0	0	0	0	0	0	0	0
1	0	2	0	0	0	2	0	0	1	3	0	0	0	0	1	0	1	0
0	2	2	0	0	0	0	0	0	1	2	0	0	0	0	0	0	0	0
0	256	0	0	0	0	0	15	0	1	0	0	23	0	0	25	0	0	0
0	37	0	0	0	0	0	125	5	0	1	0	23	5	0	49	0	0	0
0	5	29	0	0	0	3	6	0	0	8	0	0	0	0	0	0	0	1
0	17	3	0	0	3	0	10	2	0	3	0	0	0	0	26	0	0	0
0	0	21	0	0	0	0	32	0	5	14	33	0	0	0	4	0	0	0
0	0	17	0	0	0	0	9	0	0	7	9	0	1	0	4	0	0	0
0	0	32	0	0	0	1	4	1	17	35	75	0	0	1	9	0	0	1
0	6	0	0	0	0	8	0	5	10	26	0	0	0	1	0	0	4	
1	11	9	10	0	0	0	44	0	1	13	5	12	0	0	7	0	0	0
0	1	5	0	0	0	0	2	0	0	12	13	0	0	0	1	0	0	0
0	1	6	0	0	0	1	0	0	0	54	7	0	0	0	2	0	0	0
0	0	13	0	0	0	0	15	0	0	43	1	0	0	0	6	0	0	0
0	8	0	0	0	0	0	2	0	0	18	16	0	0	0	6	0	0	0
2	169	9	0	0	0	0	28	0	0	0	0	61	52	28	47	0	0	0
0	140	0	0	0	0	0	18	2	1	0	0	31	1	0	21	0	0	0
0	80	13	2	0	77	0	56	0	0	0	0	71	18	0	32	0	0	0
0	27	1	2	0	84	0	30	1	0	0	0	53	30	6	19	0	0	0
0	7	2	17	0	9	0	5	0	0	35	0	1	2	0	1	0	0	0
0	0	21	68	0	0	0	0	0	1	41	0	1	0	0	0	0	1	0
0	14	0	4	0	108	0	0	0	0	1	0	9	2	0	21	0	0	0
0	0	1	17	0	0	0	0	0	0	0	0	0	0	0	16	0	0	0
0	0	21	3	0	0	0	0	0	0	8	9	0	0	0	100	0	0	0
0	0	115	2	0	0	0	0	0	0	10	1	0	0	0	21	0	0	0
0	0	26	0	0	0	0	0	0	2	8	5	0	0	0	31	0	0	0
0	0	0	0	0	5	0	0	0	4	5	0	0	0	0	32	0	0	0
0	0	3	1	0	0	1	0	0	2	7	0	0	0	0	20	0	0	0
0	1	17	11	0	28	0	0	0	5	8	0	0	0	0	13	0	0	0
0	0	0	0	0	1	0	0	0	0	1	0	0	0	0	1	0	0	0
0	0	1	0	0	1	0	0	0	0	0	0	0	0	0	2	0	0	0
0	0	0	0	0	1	0	0	0	2	3	0	0	0	0	0	0	0	0
0	0	0	1	0	4	0	0	0	3	3	0	0	0	0	2	0	0	0
0	0	0	0	0	1	0	0	0	8	3	0	0	0	0	0	0	0	0

Appendix E. Analyses of the benthic foraminifer assemblage at Hole 681B.

Site	Core/ section	Interval (cm)	Depth (m)	Plankt. f.	Total benthic f.	*B. costata*	*B. salvad.*	*B. seminuda*	*B. denuda*	*B. margin.*	*B. curta*	*C. tumida*	*C. auka*	*E. bradyana*	*Globobul.*
681B	1H-1	23–27	0.23	14	180	44	0	97	0	0	0	21	3	0	0
681B	1H-3	23–27	4.23	33	399	177	0	183	1	0	0	0	0	0	0
681B	1H-CC	6	5.79	10	525	174	0	261	6	0	1	1	0	0	0
681B	2H-1	28–32	6.18	5	284	94	0	119	0	0	0	4	2	10	0
681B	2H-1	120–124	7.10	27	328	161	0	62	0	0	0	0	1	0	0
681B	2H-2	69–73	8.09	27	178	104	0	30	0	0	0	0	0	0	0
681B	2H-3	28–32	9.18	18	285	221	0	34	0	0	0	0	0	0	0
681B	2H-3	120–124	10.10	11	373	167	0	60	0	0	0	0	0	0	0
681B	2H-5	69–73	12.59	0	175	61	0	113	0	0	0	0	0	0	0
681B	2H-7	28–32	15.18	0	259	82	0	134	2	0	0	0	0	0	0
681B	3H-2	23–27	17.13	24	517	405	0	55	0	0	0	0	0	0	0
681B	3H-2	73–77	17.63	9	179	109	0	29	20	0	0	0	0	0	0
681B	3H-3	73–77	19.13	13	581	398	0	23	0	0	0	0	0	0	0
681B	3H-4	123–127	21.13	0	211	42	0	165	0	0	0	0	0	0	0
681B	3H-6	73–77	23.63	49	373	158	1	125	0	0	0	3	1	0	0
681B	4H-1	73–77	25.63	14	308	158	0	107	0	0	0	0	0	0	0
681B	4H-2	123–127	27.63	27	282	104	0	76	0	0	1	0	0	0	0
681B	4H-3	73–77	28.63	21	273	96	0	100	0	0	0	0	2	4	0
681B	4H-4	23–27	29.63	0	215	83	0	129	1	0	0	0	0	1	0
681B	4H-5	23–27	31.13	45	400	96	0	222	1	0	0	1	2	0	0
681B	4H-5	123–127	32.13	20	230	93	0	89	0	0	0	0	0	0	0
681B	4H-7	23–27	34.13	41	330	118	0	166	0	0	0	1	1	0	0
681B	5H-2	73–77	36.63	2	226	51	0	132	0	24	0	11	0	0	2
681B	5H-4	123–127	40.13	66	556	7	5	274	0	0	0	94	0	161	0